THE TRANSCRIPTION FACTOR NUCLEAR FACTOR ERYTHROID-2 RELATED 2 REGULATES HEMATOPOIETIC STEM CELL FUNCTION AND T-CELL ALLOREACTIVITY

A Dissertation

Presented To The Faculty Of The Weill Cornell Graduate School

Of Medical Sciences

in Partial Fulfillment Of The Requirements for the Degree Of

Doctor Of Philosophy

by

Jennifer Jia-ying Tsai

August 2016

THE TRANSCRIPTION FACTOR NUCLEAR FACTOR ERYTHROID-2 RELATED 2 REGULATES HEAMTOPOIETIC STEM CELL FUNCTION AND T-CELL ALLOREACTIVITY

Jennifer Jia-ying Tsai, MBChB (MD), Ph.D.

Cornell University 2016

Coordinating the balance between haematopoietic stem cell (HSC) quiescence and self-renewal is crucial for maintaining haematopoiesis lifelong. Equally important for haematopoietic function is modulating their localisation within their bone marrow niches, as maintenance of HSC function is tightly controlled by a complex network of intrinsic molecular mechanisms and extrinsic signalling interactions with their surrounding microenvironment. Recent findings have suggested that a common mediator of these functions is the CXCR4-CXCL12 axis. In the first part of the dissertation, we demonstrate that nuclear factor erythroid 2-related factor 2 (Nfe2l2, or Nrf2), well-established as a global regulator of oxidative stress response, plays a regulatory role in all these aspects of HSC homeostasis. Nrf2-deficiency results in an expansion of haematopoietic stem and progenitor cells (HSPCs) due to cell-intrinsic hyperproliferation, which was accomplished at the expense of HSC quiescence and self-renewal. We further show that Nrf2 mediates both migration and retention of HSCs in their niche. Moreover, we identify a previously unrecognized link between Nrf2 and CXCR4, contributing, at least partially, to the maintenance of the main modalities of HSC function.

While there is mounting evidence including ours suggesting a critical role of Nrf2 in HSC homeostasis and lymphohematopoietic malignancies, little is known about its role in T-cell biology. In the second part of the dissertation, we evaluate the relative contribution of Nrf2 to alloreactive T cells in the context of allogeneic bone marrow transplant (allo-BMT). Allogeneic bone marrow transplant (allo-BMT) is the most potent modality of cellular immune therapy for lymphohematologic malignancies. The therapeutic benefits of allo-BMT are derived from the cytoreductive conditioning, as well as the immune-mediated graft-versus-tumor (GVT) effect. However, one of the main drawbacks to the widespread use of allo-BMT is graft-versus-host disease (GVHD). Allogeneic donor T (allo-T) lymphocytes are the primary mediators facilitating both GVT and GVHD responses. We validate the biological significance of Nrf2 in T lymphocytes by showing nuclear translocation of Nrf2 upon T cell activation *in vitro*, and an increased cellular Nrf2 level specifically within $CD4^+$ donor T cells upon alloactivation *in vivo*. We demonstrate that Nrf2-deficiency in donor T cells leads to attenuated acute GVHD, which is associated with stabilization of $Helios^+$ regulatory T cells, present in the graft at the time of transplant, as well as defective upregulation of the gut homing receptor LPAM-1 of $CD8^+$ allo-T cells. However, $Nrf2^{-/-}$ donor $CD8^+$ T cells possess intact killing ability against alloantigens and A20 lymphoma cells. With their preserved GVT activity and ameliorated GVHD severity, $Nrf2^{-/-}$ donor T cells conferred an overall improved survival in the tumor-bearing allo-BMT recipients. Our findings not only characterize a novel role of Nrf2 in T cell function, but also reveal an exciting target for therapeutic manipulation as a useful clinical strategy to improve the outcomes of allo-BMT.

BIOGRAPHICAL SKETCH

Jennifer Jia-Ying Tsai was born in Taipei, Taiwan, and raised in Dunedin, New Zealand. She attended Otago Medical School, University of Otago, in Dunedin, New Zealand and graduated with a Bachelor of Medicine, Bacholor of Surgery (MBChB) in Dec 2006. The three years of clinical training in the Christchurch division of Otago Medical School as a medical student and the two years of internal medicine training as a resident in Hamilton, New Zealand encouraged her passion for hematology and immunology. Having realized the breadth and depth of potential research questions and discoveries that these fields allow for and her passion for gaining first-handed experiences in addressing these questions, the author joined the laboratory of Dr. Marcel R.M. van den Brink at Memorial Sloan-Kettering Cancer Center, New York in Nov 2008. During this time, her two mentors and role models, Dr. Marcel R.M. van den Brink and Dr. Jarrod A. Dudakov, further inspired her to pursue training in a formal and rigorous PhD program to braoden her knowledge and to further refine her research methodology. Subsequently, the author was matriculated to the Immunology & Microbial Pathogenesis Program at the Weill Cornell Graduate School of Medical Sciences to study for her Doctor of Philosophy in Jul 2011.

DEDICATION

This dissertation is dedicated to the following people:

My mother, Dr. Hsi-Huang Tseng, who has instilled in me a lifelong love of learning and inspired me to follow my passion;

My father, Dr. Wen-Yu Tsai, who has been my role model for persistence, meticulousness and conscientiousness on his career as a pediatric endocrinologist, and has always been the greatest support throughout my life;

My husband, Dr. Chou-Jui Raymond Lin, who has been my best friend for the last fifteen years and shared his unreserved support, love, patience, and many of the sacrifices for completing this dissertation.

ACKNOWLEDGMENTS

First of all, I would like to express my deepenst gratitude to my advisor, Dr. Marcel R.M. van den Brink, who has continually and successfully trained numerous physician-scientists, for generously giving me an opportunity to conduct science in his laboratory without prior bench experiences and for sparkling my interest in conducting translational research. Without his unwavering support and mentorship for his trainees and willingness to adventure in research, this dissertation would not have been possible. Secondly, I wish to extend my gratitude to my external examiner, Dr. Jarrod A. Dudakov, who was a former senior scientist in the van den Brink Laboratory and now a faculty member at the Fred Hutchinson Cancer Research Center, Seattle. Dr. Dudakov is a great thinker, an elegant writer, and a scientist with passion and practicality just like Dr. van den Brink, and together they have generated numerous stimulating discussions and constructive criticisms that have always given me the impetus to further research.

I would also like to sincerely thank my committee members, Dr. Malcolm A.S. Moore and Dr. Eric G. Pamer, for all their valuable scientific advice and knowledge and the insightful discussions and suggestions during committee meetings. In addition, a big thank you to Dr. Joseph Sun, the chairperson of my thesis defense and my Admission-to-Candidacy Examination, for sharing his experiences and helpful career advice in general.

I wish to acknowledge the support received from the staff and colleages in both the Weill Cornell Graduate School of Medical Sciences and the Memorial Sloan-Kettering Cancer Cancer communities. Additionally, I would like to thank all my-coauthors for sharing my research path with me and for contributing to my thesis work. I am particularly grateful to Dr. Amanda M. Holland, Dr. Enrico Velardi, and Dr. Yusuke Shono for sharing my pain and joy in this journey, for providing numerous intellectual inputs and various forms of support during my graduate study, and for helping me stay sane through these difficult years. I also wish to take the opportunity to thank my funding agents, the Cancer Research Institute Tumor Immunology Predoctoral Fellowship and the Sloan Kettering Institute Dorris J. Hutchison Student Fellowship for their generous support.

Finally, I would like to express my heart-felt gratitude to my family, to whom this dissertation is dedicated. Their love, patience, understanding and support all these years have encouraged me to follow my passion, to adventure in off-the-beaten paths, and to preservere in spite of overwhelming obstacles.

TABLE OF CONTENTS

Title page	i
Copyright page	ii
Abstract	
Biographical Sketch	iii
Dedication	iv
Acknowledgments	v
Table of Contents	vii
List of Figures	viii
Chapter 1. Introduction	1
Chapter 2. Nrf2 Regulates Hematopoietic Stem Cell Function	6
Chapter 3. Nrf2 Regulates T-cell Alloreactivity	28
Chapter 4. Discussion	50
Chapter 5. Materials and Methods	57
Chapter 6. References	65

LIST OF FIGURES

Figure 1.1 *Nrf2*$^{-/-}$ Mice Exhibit an Expanded Haematopoietic Stem and Progenitor Pool.

Figure 1.2 Rapid Proliferation and Differentiation of *Nrf2*$^{-/-}$ HSPCs *in vitro*.

Figure 1.3 Nrf2 Regulates HSPC Proliferation and Differentiation Intrinsically.

Figure 1.4 Nrf2 Controls LT-HSC Proliferation and Differentiation.

Figure 1.5. Nrf2 Maintains HSC Quiescence.

Figure 1.6 Nrf2 Sustains HSC Self-renewal.

Figure 1.7 Nrf2 Governs HSPC Retention and Migration to BM Niche.

Figure 1.8 Reduced CXCR4 Expression in *Nrf2*$^{-/-}$ HSPCs.

Figure 1.9 Nrf2 Regulates Cxcr4 Promoter.

Figure 1.10 Nrf2 Mediates HSPC Functions Through CXCR4.

Figure 2.1 T Cell Activation Promotes Nrf2 Nuclear Translocation and Protein Expression.

Figure 2.2 *Nrf2*$^{-/-}$ T Cells Induces Less GVHD Mortality and Morbidity.

Figure 2.3 *Nrf2*$^{-/-}$ Donor T Cells Results in Less Hepatic, Intestinal, and Thymic GVHD.

Figure 2.4 *Nrf2*$^{-/-}$ T Cells Display Intact Proliferation, Activation, and Survival.

Figure 2.5 *Nrf2*$^{-/-}$ Donor T Cells Display Decreased Intestinal Infiltration and LPAM-1 Expression

Figure 2.6 Nrf2 Ablation Alters Donor CD4^{+} T Cell Compartmentalization

Figure 2.7 Nrf2 is Dispensible for Induction of Tregs *in vitro*.

Figure 2.8 Abrogation of GVHD in *Nrf2*$^{-/-}$ allo-T cell recipients is associated with a greater proportion of donor-derived CD4^{+} Helios^{+} Tregs.

Figure 2.9 WT and *Nrf2*$^{-/-}$ Tregs under steady-state do not differ before transplantation

Figure 2.10 Nrf2 Is Dispensible for Donor CD8^{+} T-Cell Cytotoxicity and GVT Capacity.

CHAPTER ONE

Introduction

Hematopoiesis

Hematopoiesis is supported by HSCs that are fundamentally characterized by their ability to self-renew and potency to differentiate into all blood lineages. Postnatally the most quiescent HSCs reside in a relatively hypoxic microenvironmental niche in the bone marrow[1,2] and are capable of sustaining lifelong hematopoiesis. Maintenance of HSC functions, including their localization, quiescence, self-renewal, and differentiation, is finely regulated by a complex network of intrinsic molecular mechanisms and extrinsic signaling interactions with their surrounding microenvironment (Kiel and Morrison, 2008). The interaction between the chemokine receptor CXCR4, expressed on the surface of HSCs, and its ligand CXCL12, produced by the bone marrow niche, has been well described as regulating homing, localization and retention of HSCs in their niche. Moreover, recent studies have demonstrated that conditional deletion of CXCR4 or CXCL12 in young adult mice leads to hyperproliferation of hematopoietic stem and progenitor cells (HSPCs) at the expense of HSC quiescence and self-renewal (Nie et al., 2008; Sugiyama et al., 2006; Tzeng et al., 2011), demonstrating the complex linkages in the main modalities of HSC function.

In addition to these extrinsic cues that regulate HSC function, mounting evidence supports an essential role for intracellular redox balance in maintaining stem cell quiescence and stemness. Previous studies indicate that low oxygen concentration is critical for maintaining stem cell quiescence in various tissues (Ezashi et al., 2005; Mazumdar et al., 2010; Yun et al., 2005; Yun et al., 2002), including the bone marrow niche (Takubo et al., 2010). Reactive oxygen species (ROS), natural metabolites of oxygen under physiological conditions, have recently been shown to prime HSPCs for differentiation in *Drosophila* (Owusu-Ansah and Banerjee, 2009). In mouse models, disruption of oxidative stress pathways leads to premature HSC senescence due to loss of HSC quiescence and decline in the capacity for self-renewal (Ito et al., 2004; Ito et al., 2006; Tothova et al., 2007). Taken together, these findings indicate that modulation of the redox balance plays a pivotal role in maintaining HSC functions.

The Transcription Factor Nrf2

Nuclear factor erythroid 2-related factor 2 (Nfe2l2, or Nrf2) belongs to the "cap-n-collar" subfamily of the basic leucine zipper (b-Zip) transcription factors (Moi et al., 1994), and is a master regulator in the antioxidant response pathway (Li and Kong, 2009; Nguyen et al., 2009). In the basal resting state, Nrf2 is constitutively expressed but rendered inactive by sequestration in the cytosol by the cytoskeleton-associated protein, Kelch-like ECH-associated protein 1 (Keap1) (Itoh et al., 1999). In response to oxidative stress, Nrf2 translocates from the cytosol into the nucleus and binds to Antioxidant Response Element (ARE), a cis-acting DNA regulatory element located in the upstream promoter region of many

genes encoding for Phase II detoxifying and antioxidant enzymes, where it drives their transcription (Itoh et al., 1997). The resultant induction of Nrf2 target genes therefore provides an essential mechanism for cellular defense against oxidative stress.

Nrf2 and Hematopoiesis

Despite its ubiquitous expression in all tissues, Nrf2 was found to be dispensable for murine development, growth and erythropoiesis (Chan et al., 1996). Dual roles of Nrf2 have been observed in its regulation in differentiation in various tissues. While Nrf2 was found to promote differentiation of neuronal cells and adipocytes (Pi et al., 2010; Zhao et al., 2009), it was also reported to inhibit differentiation of chondrocytes and osteoblasts (Hinoi et al., 2006; Hinoi et al., 2007). Due to the continual requirement for HSC protection from oxidative stress, along with recent findings that Nrf2 maintains homeostatic quiescence of intestinal stem cells in *Drosophila* (Hochmuth et al., 2011), we sought to assess the role of Nrf2 in regulating HSPC functions.

Allogeneic Bone Marrow Transplant

Allogeneic bone marrow transplant (allo-BMT) is the most potent modality of cellular immune therapy for hematologic malignancies and certain metastatic solid tumors. The therapeutic benefits of allo-BMT are derived from the high dose of cytoreductive conditioning, as well as the immune-mediated graft-versus-tumor (GVT) effect. However, the flip side to the beneficial effects of GVT is acute

graft-versus-host disease (GVHD), which is a systemic inflammatory disease characterized by profound immunosuppression and host tissue damage affecting up to 40-60% of allo-BMT patients and accounting for 15% of deaths after allo-BMT[3], limiting the success and wider application of allo-BMT despite its curative potential for malignancies refractory to all other treatments. Allogeneic donor T lymphocytes are the primary mediators facilitating both GVT and GVHD responses[4]. It is therefore not surprising that separation of the undesired GVHD and beneficial GVT activities of allo-T cells has attracted intense research pursuits, and remains paramount for improving clinical outcomes in patients with malignancies treated with allo-BMT.

Nrf2 and T-cell Alloreactivity

Nuclear factor erythroid-derived 2-like 2 (NFE2L2, or Nrf2) is a ubiquitously expressed basic leucine zipper transcription factor well-established as a master regulator of cellular redox, detoxification, and stress pathway. The dual roles of Nrf2 in cancer promotion and cancer prevention in various solid tumors have been widely studied for its importance in tumorigenesis[5,6]. Moreover, we and others have recently shown that Nrf2 positively regulates the self-renewal ability of hematopoietic stem cells[7]. Consistent with our findings, high levels of Nrf2 expression have been identified in various hematologic malignancies[8-13]. It has also been proposed that the increased activity of Nrf2 underlies the chemoresistance of leukemia/lymphoma cells to apoptosis. Although previous studies have implicated the involvement of Nrf2 in T cell activation *in vitro*, detailed characterization of its role in T cell function *in vivo* is still lacking [14-16].

While inhibition of Nrf2 pathway represents a rational therapeutic approach against hematologic malignancies, we investigated its impact on allo-BMT, the definitive curative antitumor therapy for the majority of hematologic cancers. Specifically, we hypothesized that Nrf2 may be involved in T-cell alloreactivity and cytotoxicity. In this study, we sought to methodically analyze the effects of Nrf2 disruption in donor T cells on their abilities to proliferate, to activate, to polarize, to kill, and ultimately to cause GVHD and GVT using genetically altered *Nrf2*$^{-/-}$ mice.

CHAPTER TWO

Nrf2 Regulates HSC Function

Nrf2$^{-/-}$ Mice Exhibit an Expanded Haematopoietic Stem and Progenitor Pool

To determine whether Nrf2 plays a role in haematopoiesis, we first quantified the primitive HSPCs in *Nrf2*$^{-/-}$ mice in steady-state conditions. In young adult Nrf2-deficient animals, we observed an increase in both percentage and absolute number of LSK (Lineage^{-}Sca-1^{+}c-Kit^{+}) cells compared to age-matched *Nrf2*$^{+/+}$ wild-type (WT) controls (**Figure 1.1 a, b**), although overall BM cellularity was unchanged (data not shown). More comprehensive analysis of the LSK fraction revealed significant increases at the short-term HSC (ST-HSC, CD34^{+}Flt3^{-}) and continued through multipotent progenitor (MPP, CD34^{+}Flt3^{+}) stages, but did not impact on long-term HSCs (LT-HSC, CD150^{+}CD48^{-}CD34^{-}Flt3^{-}) (**Figure 1.1 c**). We also found increases in the number of committed downstream progenitors of both the myeloid and lymphoid lineages (**Figure 1.1 d, e**). Consistent with these findings, we also observed significantly increased colony formation from *Nrf2*$^{-/-}$ BM in cobblestone area-forming cell (CAFC) and colony-forming cell (CFC) assays (**Figure 1.1 f, g**). Together, these results suggest that loss of functional Nrf2 leads to expansion of the haematopoietic progenitor pool but spares the most primitive LT-HSCs.

Figure 1.1 Nrf2$^{-/-}$ Mice Exhibit an Expanded Haematopoietic Stem and Progenitor Pool

WT and Nrf2$^{-/-}$ bone marrow (BM) under steady-state were examined from 8-10 week old female mice. ***(a)*** *Representative flow cytometric analysis comparing WT to Nrf2$^{-/-}$ LSK frequency, gated on lineage^{-} (Lin^{-}) cells.* ***(b - e)*** *Absolute number of LSK cells* ***(b)****, HSC subsets* ***(c)****, myeloid progenitors* ***(d)*** *or lymphoid progenitors* ***(e)****, mean ± SEM of data from 8 animals per strain over 2 independent experiments. CMP, Common myeloid progenitor (Lin^{-}c-kit^{+}Sca-1^{-} CD34^{+}CD16/32^{mid}); GMP, Granulocyte-macrophage progenitor (Lin^{-}c-kit^{+}Sca-1^{-} CD34^{+}CD16/32^{high}); MEP, Megakaryocyte-erythroid progenitor (Lin^{-}c-kit^{+}Sca-1^{-} CD34^{-}CD16/32^{low}); LMPP, Lymphoid-primed multipotent progenitor (Lin^{-}c-kit^{+}Sca-1^{+}CD34^{+}Flt3^{+}CD62L^{high}); CLP, Common lymphoid progenitor (CLP-1: Lin^{-}IL-7Ra^{+}c-kit^{+}; CLP-2: Lin^{-}IL-7Ra^{+}B220^{+}).* ***(f)*** *Number of colonies formed from WT or Nrf2$^{-/-}$ BM in cobblestone area-forming cells assay (CAFC), mean ± SEM of data from 11 animals per strain over 3 independent experiments. MNCs, Mononucleated cells.* ***(g)*** *Number of colonies formed from WT or Nrf2$^{-/-}$ BM in myeloid (CFU-GM), erythroid (BFU-E), and mixed (CFU-Mix) lineages in colony-forming cell assay (CFC), data represent mean ± SEM from 13 WT and 12 Nrf2$^{-/-}$ mice over 3 independent experiments.*

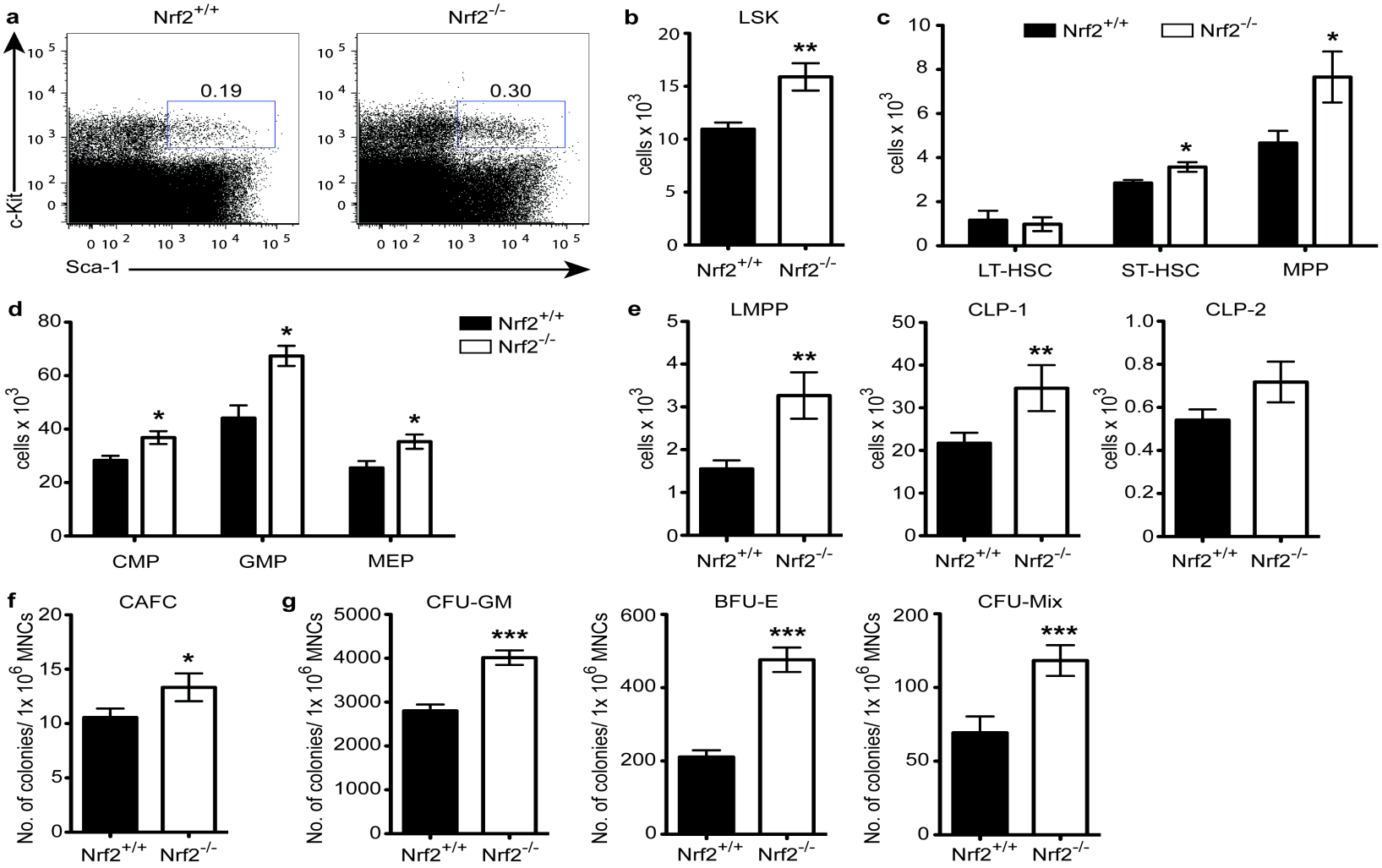
a
Nrf2+/+
Nrf2-/-
0.19
0.30
c-Kit
Sca-1
b
LSK
cells x 10^3
Nrf2+/+
Nrf2-/-
c
Nrf2+/+
Nrf2-/-
cells x 10^3
LT-HSC
ST-HSC
MPP
d
Nrf2+/+
Nrf2-/-
cells x 10^3
CMP
GMP
MEP
e
LMPP
CLP-1
CLP-2
cells x 10^3
Nrf2+/+
Nrf2-/-
f
CAFC
No. of colonies/ 1x 10^6 MNCs
Nrf2+/+
Nrf2-/-
g
CFU-GM
BFU-E
CFU-Mix
No. of colonies/ 1x 10^6 MNCs
Nrf2+/+
Nrf2-/-

Nrf2 Regulates HSPC Proliferation and Differentiation Intrinsically

To test the impact of Nrf2 on HSPC function, we co-cultured sorted LSK cells from *Nrf2*$^{-/-}$ (CD45.2) and WT (CD45.1) BM in a competitive setting on OP9-DL1 culture, which allows the *in vitro* analysis of T cell development from HSPCs. As expected given their increased number *in vivo* (**Figure 1.1**), even when seeded in equal numbers, *Nrf2*$^{-/-}$ LSKs dominated the culture as early as day 3 (**Figure 1.2, a, b**), indicating a competitive advantage in proliferation as a result of Nrf2 deficiency. T cell development progresses through a series of distinct stages that can be identified based on their differential expression of CD4, CD8, CD25 and CD44 [17]. In addition to their enhanced proliferation, we also observed that *Nrf2*$^{-/-}$ LSKs had enhanced differentiation kinetics compared to WT controls (**Figure 1.2, c, d**), rapidly progressing to the DN2 ($CD4^{-}CD8^{-}CD44^{+}CD25^{+}$) and DN3 ($CD4^{-}CD8^{-}CD44^{-}CD25^{+}$) stages. Moreover, we found significantly increased expression of Ki-67 on LSKs from *Nrf2*$^{-/-}$ compared with WT BM *in vivo* (**Figure 1.2, e**), in concordance with the enhanced proliferation observed *in vitro*.

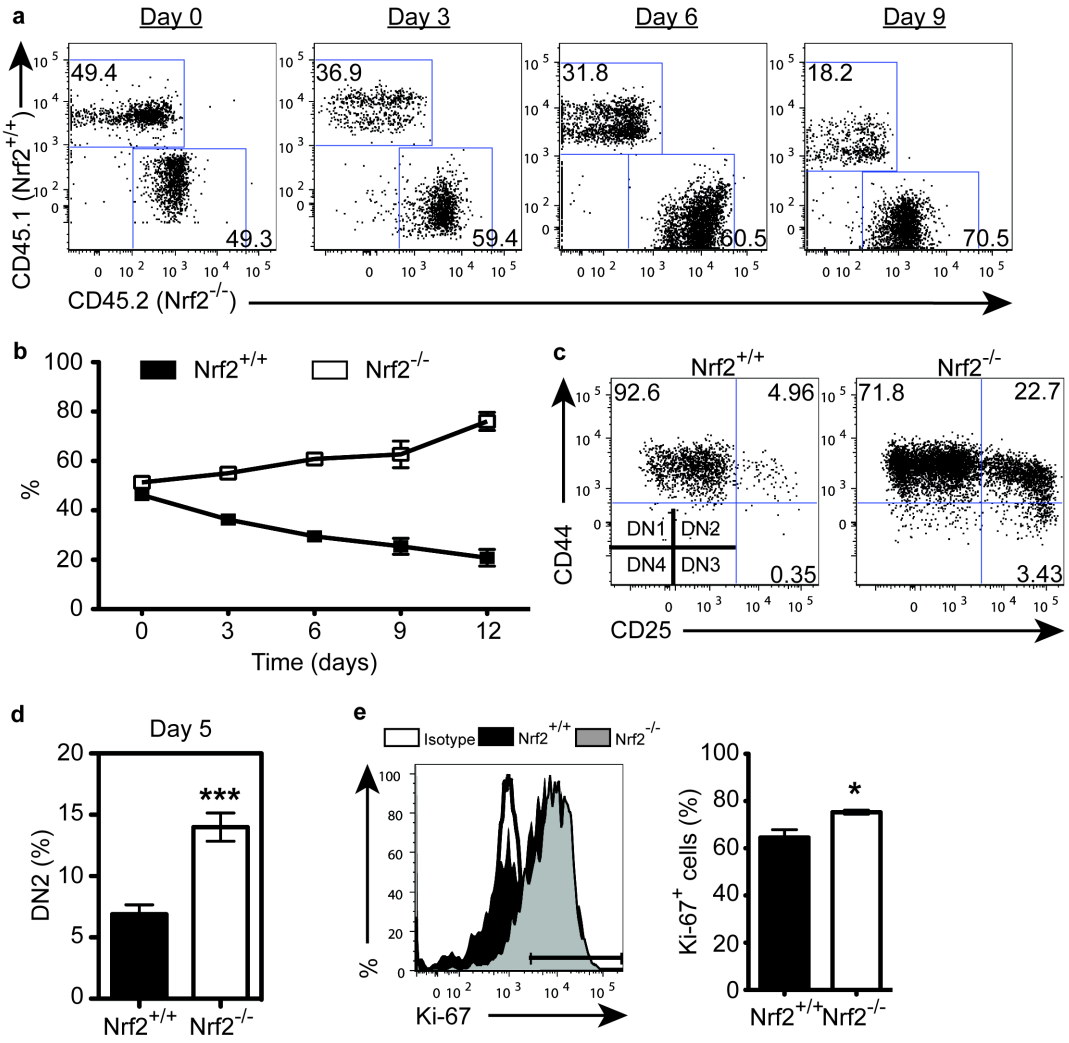

Figure 1.2. Rapid Proliferation and Differentiation of Nrf2$^{-/-}$ HSPCs in vitro

*Sorted BM LSK cells were seeded onto OP9-DL1 stromal cells. (**a-b**) Relative contribution of Nrf2$^{-/-}$ (CD45.2) and WT (CD45.1) cells when co-cultured at a 1:1 ratio on day 0; (**c**) Differentiation of WT or Nrf2^{-} LSKs cultured for 5 days, gated on double-negative (DN, CD4^{-}CD8^{-}) population, and (**d**) Percentage of LSKs differentiating into DN2 stage on day 5. (**a-d**) Data represent the mean ± SEM, n = 7 independent observations over 4 experiments. (**e**) Expression of Ki-67 in WT and Nrf2$^{-/-}$ BM LSKs, representative plot (left) and bar graph (right) showing mean ± SEM of 4 animals per strain over 2 independent experiments.*

Given the ubiquitous expression of Nrf2, it is essential to clarify whether these differences in HSPC proliferation and differentiation kinetics are caused extrinsically by the BM niche or intrinsically by the HSPC itself. To assess the role of the BM niche, we generated chimeras using CD45.1^{+} WT LSKs transferred into either CD45.2^{+} WT or CD45.2^{+} *Nrf2*$^{-/-}$ hosts. After 8 weeks, which allowed for effective primary reconstitution, we sorted LSKs from these chimeric mice and co-cultured them with OP9-DL1 stromal cells. Transplanted CD45.1^{+} WT LSKs behaved in a similar manner irrespective of their pre-conditioning microenvironment (**Figure 1.3, a - d**). In contrast, when we performed the reciprocal chimeric experiment where CD45.2^{+} WT or CD45.2^{+} *Nrf2*$^{-/-}$ LSKs, previously primed in CD45.1^{+} WT hosts, were co-cultured on OP9-DL1 stromal cells, we discovered once again that transplanted CD45.2^{+} *Nrf2*$^{-/-}$ LSKs proliferated more and differentiated faster than transplanted *Nrf2*$^{+/+}$ WT LSKs (**Figure 1.3, e - h**). Taken together, these results suggest that Nrf2 regulates proliferation and differentiation of HSPCs in a cell-intrinsic manner.

Figure 1.3. Nrf2 Regulates HSPC Proliferation and Differentiation Intrinsically

*(**a** - **d**) CD45.1^{+} WT LSKs were preconditioned in CD45.2^{+} WT or Nrf2$^{-/-}$ animals in vivo then seeded onto OP9-DL1 with untransplanted CD45.2^{+} WT LSKs at a 1:1 ratio on day 0. (**a**) Relative contribution of cells and (**c**) percentage of preconditioned CD45.1^{+} WT LSKs at day 12 in culture. Data represent the mean ± SEM, n = 5 observations per strain over 2 independent transplant experiments. (**b**) T-cell differentiation kinetics and (**d**) percentage of CD45.1^{+} preconditioned WT LSKs differentiating into DN2 stage at day 6 in culture. Data represent the mean ± SEM, n = 10 observations from WT and 8 from Nrf2$^{-/-}$ hosts over 2*

*independent transplant experiments. (**e** - **h**) CD45.2^{+} WT or Nrf2$^{-/-}$ LSKs were preconditioned in CD45.1^{+} WT animals in vivo then seeded onto OP9-DL1 with untransplanted CD45.1^{+} WT LSKs at a 1:1 ratio at day 0. (**e**) Relative contribution of cells and (**g**) percentage of preconditioned CD45.2^{+} WT or Nrf2$^{-/-}$ LSKs at day 12 of culture. Data represent the mean ± SEM, n = 10 observations from WT and 8 from Nrf2$^{-/-}$ donors over 2 independent transplant experiments. (**f**) T-cell differentiation kinetics and (**h**) percentage of CD45.2^{+} preconditioned WT or Nrf2$^{-/-}$ LSKs differentiating into DN2 stage at day 6 in culture. Data represent the mean ± SEM, n = 9 observations from WT and 8 from Nrf2$^{-/-}$ donors over 2 independent transplant experiments.*

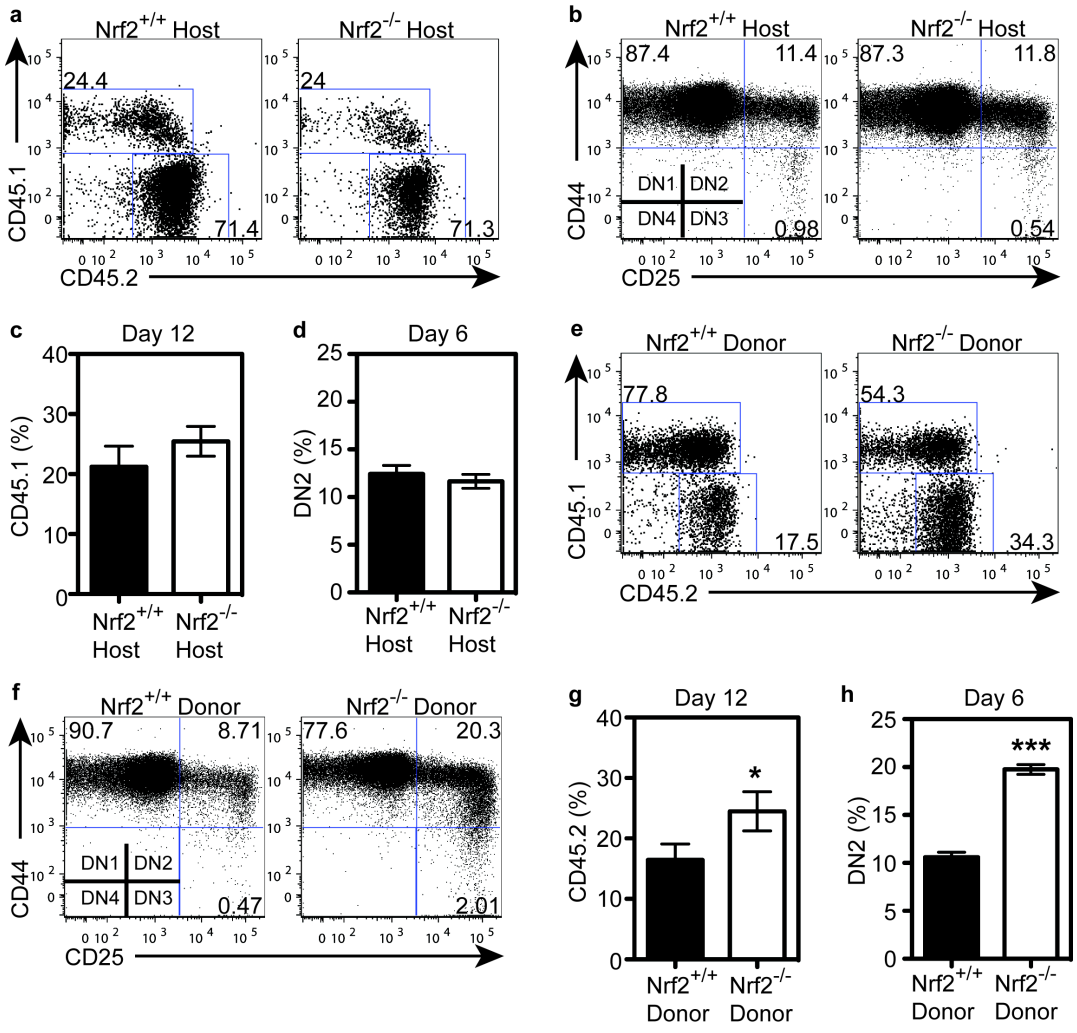

Nrf2 could be found at the transcript level in both LT-HSCs as well as their downstream MPPs (**Figure 1.4, a**), suggesting that despite their unaltered frequency in deficient animals (**Figure 1.1, c**), Nrf2 could act on this earliest haematopoietic population. Consistent with our findings on the bulk LSK cells, we found a greater proportion of *Nrf2*$^{-/-}$ LT-HSCs expressed Ki-67 (**Figure 1.4, b**), indicating that more HSCs were undergoing proliferation. Functionally, Nrf2-deficient LT-HSCs differentiated more rapidly on OP9-DL1 culture than WT controls (**Figure 1.4, c, d**). These data demonstrate that Nrf2 plays an important role in HSPC proliferation and differentiation starting at the LT-HSC stage.

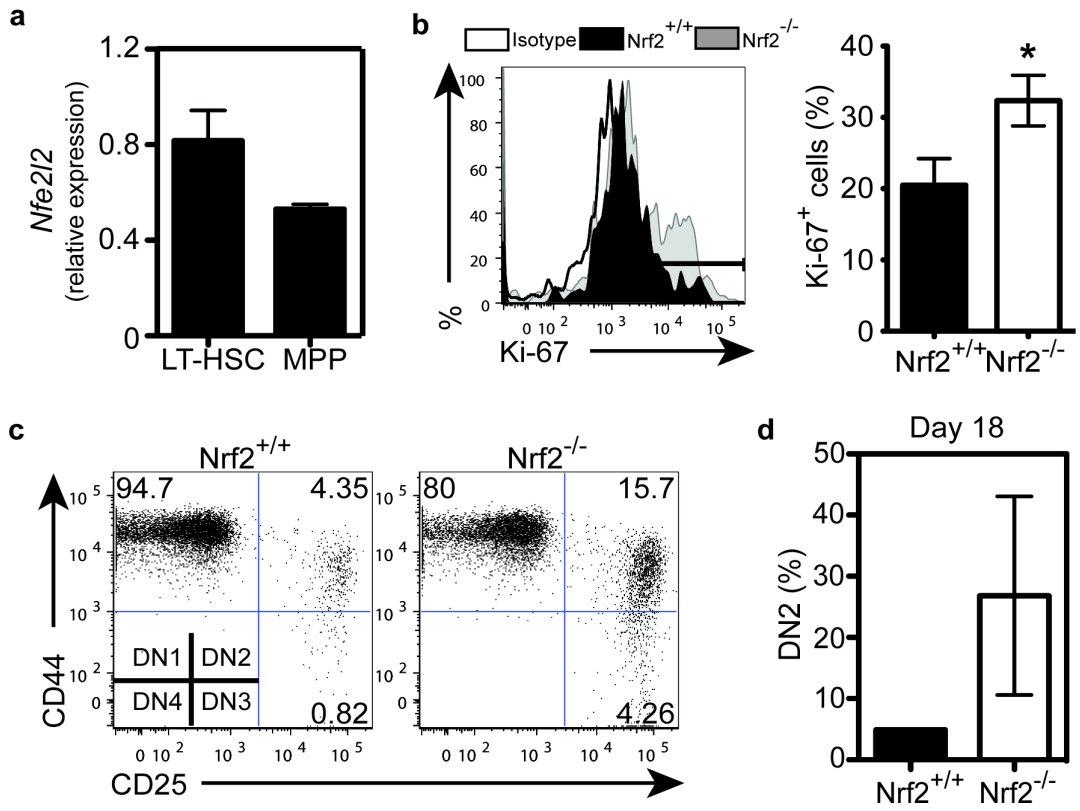

Figure 1.4. Nrf2 Controls LT-HSC Proliferation and Differentiation

*(**a**) Expression of Nfe2l2 mRNA transcripts in sorted WT LT-HSC and MPP, presented relative to Actb expression. Data represent the mean ± SEM, n = 3 independent experiments. (**b**) Expression of Ki-67 in WT and Nrf2$^{-/-}$ BM LT-HSCs, representative plot (left) and bar graph (right) showing mean ± SEM of 4 animals per strain over 2 independent experiments. (**c**) Differentiation of WT or Nrf2$^{-/-}$ LT-HSCs (**d**) percentage of LT-HSCs differentiating into DN2 stage at day 18 of OP9-DL1 co-culture system. Data represent the mean ± SEM, n = 2 independent observations from WT and 3 from Nrf2$^{-/-}$ animals over 2 experiments.*

Nrf2 Maintains HSC Quiescence and Self-Renewal

Based on these findings, we hypothesised that Nrf2 functions as a negative regulator of cell cycle entry in HSCs, actively maintaining the balance between HSC quiescence and self-renewal. As the synthesis of cyclin D is initiated during G1 phase, and its presence is required for the transition to S phase, we first assessed the level of cyclin D expression as an indirect measure of quiescence in the bone marrow. We found a 2-fold increase in cyclin $D1^{+}$ cells in the *Nrf2*$^{-/-}$ BM (**Figure 1.5, a, b**), and higher levels of cyclin D at the transcript level in purified *Nrf2*$^{-/-}$ LSKs (**Figure 1.5, c**). Furthermore, by analyzing RNA and DNA contents using Pyronin Y and Hoeschst 33342, we found fewer LSKs from *Nrf2*$^{-/-}$ BM in the quiescent G0 state (**Figure 1.5, d**), and importantly also reduced proportion of the most primitive LT-HSCs in G0 stage (**Figure 1.5, e**). These findings support our hypothesis that Nrf2 acts as a negative regulator of cell cycle progression, thereby maintaining HSC quiescence. To further explore this phenomenon *in vivo*, we exploited the characteristic of 5-Fluorouracil (5-FU), which kills cycling cells and spares quiescent stem cells. Following a single dose of 5-FU, we observed a profound reduction in the number of LT-HSCs in Nrf2$^{-/-}$ mice compared to WT controls (**Figure 1.5, f**). These findings suggest that the HSC compartment of *Nrf2* deficient mice is considerably less quiescent than WT controls.

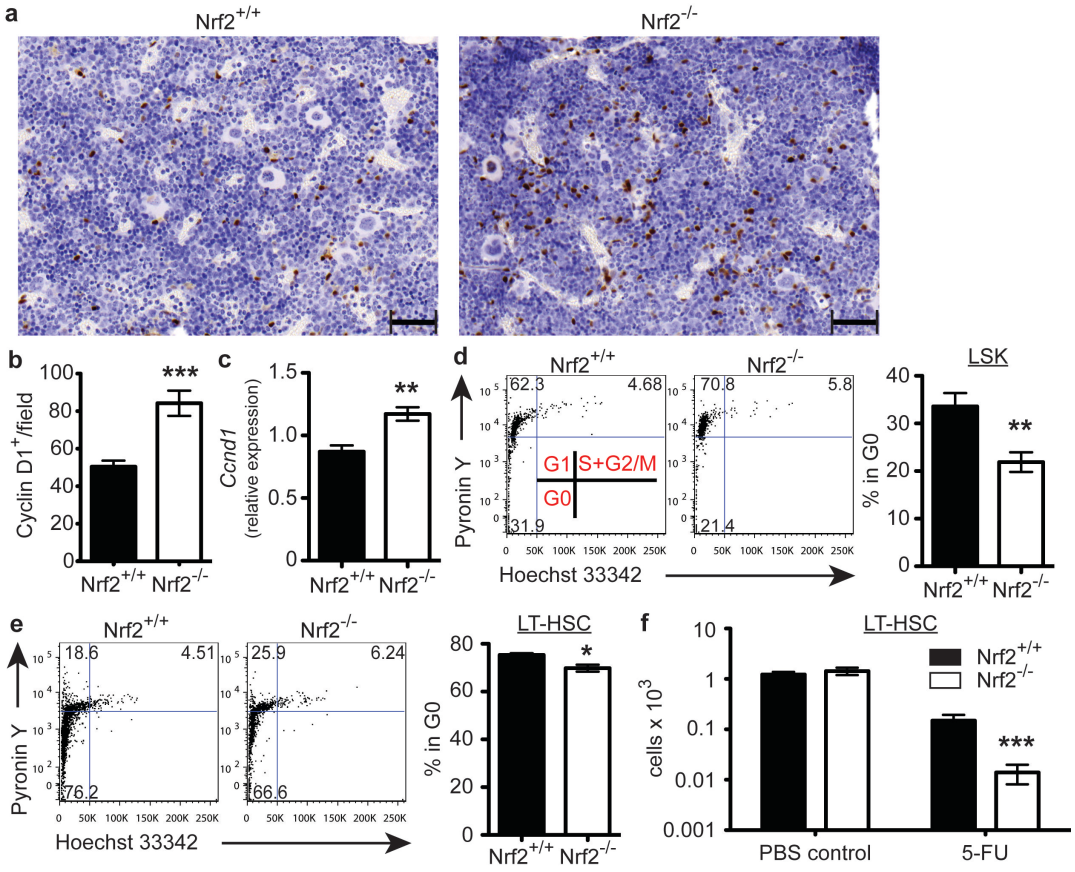

Figure 1.5. Nrf2 Maintains HSC Quiescence

*(**a**) Representative immunohistochemistry images and (**b**) Quantification of Cyclin D^+ cells in WT and $Nrf2^{-/-}$ BM sections. Data represent mean ± SEM of 8 animals per strain. (**c**) Expression of Ccnd1 mRNA transcripts in WT and $Nrf2^{-/-}$ LSKs, relative to Actb expression. Data represent mean ± SEM of 4 WT and 3 $Nrf2^{-/-}$ animals. (**d**) Representative flow cytometric analysis (Left panel) showing cell cycle status of WT and $Nrf2^{-/-}$ LSKs and bar graph (Right panel) showing the percentage of cells in the quiescent G0 phase. Data represent mean ± SEM of 5 WT and 6 $Nrf2^{-/-}$ animals. (**e**) Representative flow cytometric analysis (Left panel) showing cell cycle status of WT and $Nrf2^{-/-}$ LT-HSCs and bar graph (Right panel) showing the percentage of cells in the quiescent G0 phase. Data represent mean ± SEM of 4 animals per strain.*

Given the hyperproliferation of *Nrf2*$^{-/-}$ HSCs, coupled with the reduction of HSC quiescence, continued insult should lead to accelerated haematopoietic exhaustion. Consistent with our hypothesis, *Nrf2*$^{-/-}$ mice challenged with sequential 5-FU treatment, died significantly earlier than WT controls (**Figure 1.6, a**). To directly assess whether *Nrf2* controls the self-renewal ability of HSCs, in addition to maintaining HSPC quiescence, we performed sequential CAFC assay *in vitro* and serial competitive transplantation *in vivo*. In both the secondary plating and transplantation, we saw a dramatic reduction in the contribution of *Nrf2*$^{-/-}$ HSCs (**Figure 1.6, b, c**). Taken together, our data demonstrate that Nrf2 plays an important role in maintaining the balance between HSC quiescence and self-renewal.

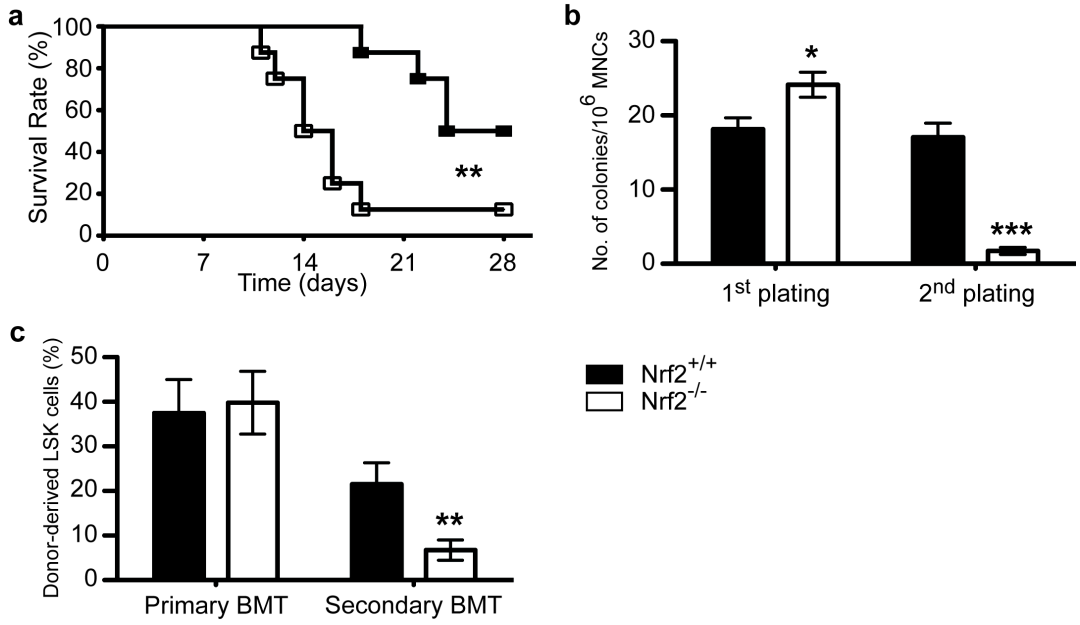

Figure 1.6. Nrf2 Sustains HSC Self-renewal

*(**a**) Survival of WT and Nrf2$^{-/-}$ mice following sequential 5-FU treatment, n = 8 animals per strain over 2 independent experiments. (**b**) Bar graphs showing colony formation in serial CAFC assays, mean ± SEM of 8 animals per strain over 3 independent experiments. (**c**) Equal numbers of donor CD45.2^{+} (WT or Nrf2$^{-/-}$) and competitor CD45.1^{+} (WT) LSK cells from BM were serially transplanted into lethally irradiated CD45.1^{+} (WT) recipients. Contribution of donor-derived (CD45.2^{+}) BM LSKs was assessed 4 months after primary and secondary bone marrow transplants (BMT). Data represent the mean ± SEM of 12 recipients of WT and 14 recipients of Nrf2$^{-/-}$ donor cells in primary transplant and 9 recipients of WT and 10 recipients of Nrf2$^{-/-}$ donor cells in secondary transplant over 2 independent experiments.*

Nrf2 Governs HSPC Retention and Migration to the Bone Marrow Niche

Interestingly, in the steady-state, *Nrf2*$^{-/-}$ mice displayed a significantly higher frequency and absolute number of HSPCs in the spleen (**Figure 1.7, a**). Consistent with this finding, *Nrf2*$^{-/-}$ splenocytes gave rise to significantly more CFU-GM and BFU-E colonies in CFC assays, and sorted *Nrf2*$^{-/-}$ splenic LSKs mimicked their BM counterparts and once again differentiated more rapidly when co-cultured with OP9-DL1 stromal cells (**Figure 1.7, a, b**). To address whether this increase in peripheral LSKs was due to a cell-intrinsic defect in HSPC retention, we generated chimeras with sorted CD45.2^{+} WT or *Nrf2*$^{-/-}$ LSKs transplanted into CD45.1^{+} WT hosts. After 8 weeks following transplant, we found significantly fewer *Nrf2*$^{-/-}$ LSKs in the BM and drastically more in the periphery (**Figure 1.7, d – g**). To explore the homing capacity, we labelled purified lineage-depleted (Lin^{-}) BM cells from CD45.1^{+} WT and CD45.2^{+} WT or *Nrf2*$^{-/-}$ mice with fluorescent dyes, injected them into lethally irradiated WT recipients, and quantified the contribution of cells present in the recipient BM 18 hours after transplant by flow cytometry. We observed that *Nrf2*$^{-/-}$ Lin^{-} BM cells trafficked to the bone marrow niche less efficiently than CD45.2^{+} WT controls (**Figure 1.7, h, i**), implying that Nrf2 is required for efficient homing of BM cells. To specifically examine the impact of Nrf2 on the homing of HSCs, we labelled and mixed WT and *Nrf2*$^{-/-}$ BM at 1:1 ratio, and compared the engraftment efficiency of the LT-HSCs 16 hours after transplant. Although present at equal numbers in the inoculum, *Nrf2*$^{-/-}$ LT-HSCs showed a significant impairment in BM engraftment, indicating a defect in their homing ability (**Figure 1.7, j, k**). Collectively, these findings suggest that Nrf2 governs the retention of HSCs and their homing to the BM niche.

Figure 1.7. Nrf2 Governs HSPC Retention and Migration to BM Niche

*(**a**) Absolute number of LSK cells in untreated spleen; mean ± SEM of 13 WT and 14 Nrf2$^{-/-}$ animals over 4 independent experiments. (**b**) Splenocytes were cultured in CFC conditions and colonies were scored for myeloid and erythroid lineages; mean ± SEM of 9 WT and 8 Nrf2$^{-/-}$ animals over 2 independent experiments. (**c**) LSK cells were isolated from spleen and co-cultured for 11 days with OP9-DL1 stromal cells, representative plots of 2 independent experiments. (**d - g**) CD45.2^{+} WT or Nrf2$^{-/-}$ LSKs were transplanted into lethally irradiated CD45.1^{+} WT recipients. Retention in the BM niche was assessed 8 weeks post-BMT. (**d**) Representative flow cytometric analysis and (**e**) quantification of WT or Nrf2$^{-/-}$ LSKs retained in the WT BM; mean ± SEM of 10 recipients of WT and 8 recipients of Nrf2$^{-/-}$ LSKs over 2 independent experiments. (**f**) Representative flow cytometric analysis and (**g**) quantification of WT or Nrf2$^{-/-}$ LSKs mobilised to the WT spleen; mean ± SEM of 10 recipients of WT and 8 recipients of Nrf2$^{-/-}$ LSKs over 2 independent experiments. (**h - i**) Equal numbers of CFSE^{+} (CD45.1^{+} WT) and Violet^{+} (CD45.2^{+} WT or Nrf2$^{-/-}$) Lin^{-} BM cells were transplanted into lethally irradiated CD45.1^{+} WT recipients and BM content was assessed 18 hours post-transplant. Representative flow cytometric analysis (**h**) and bar graphs (**i**) of WT or Nrf2$^{-/-}$ Lin^{-} BM cells. Homing efficiency = absolute number of dye^{+} Lin^{-} cells engrafted ÷ absolute number of dye^{+} Lin^{-} cells transplanted; mean ± SEM of 10 recipients per strain over 2 independent experiments. (**j - k**) Equal numbers of Violet^{+} (CD45.2^{+} WT) and CFSE^{+} (CD45.2^{+} Nrf2$^{-/-}$) BM cells were transplanted into lethally irradiated CD45.2^{+} WT recipients, and content of LT-HSCs was assessed 16 hours post-transplant. Representative flow cytometric analysis (**j**) and*

*bar graphs (**k**) showing the proportion of dye^{+} LT-HSCs in the pre-transplant mix (Left panel, pre-BMT) and in recipients 16 hours post-transplant (Right panel, post-BMT); mean ± SEM of 16 recipients per strain over 3 independent experiments.*

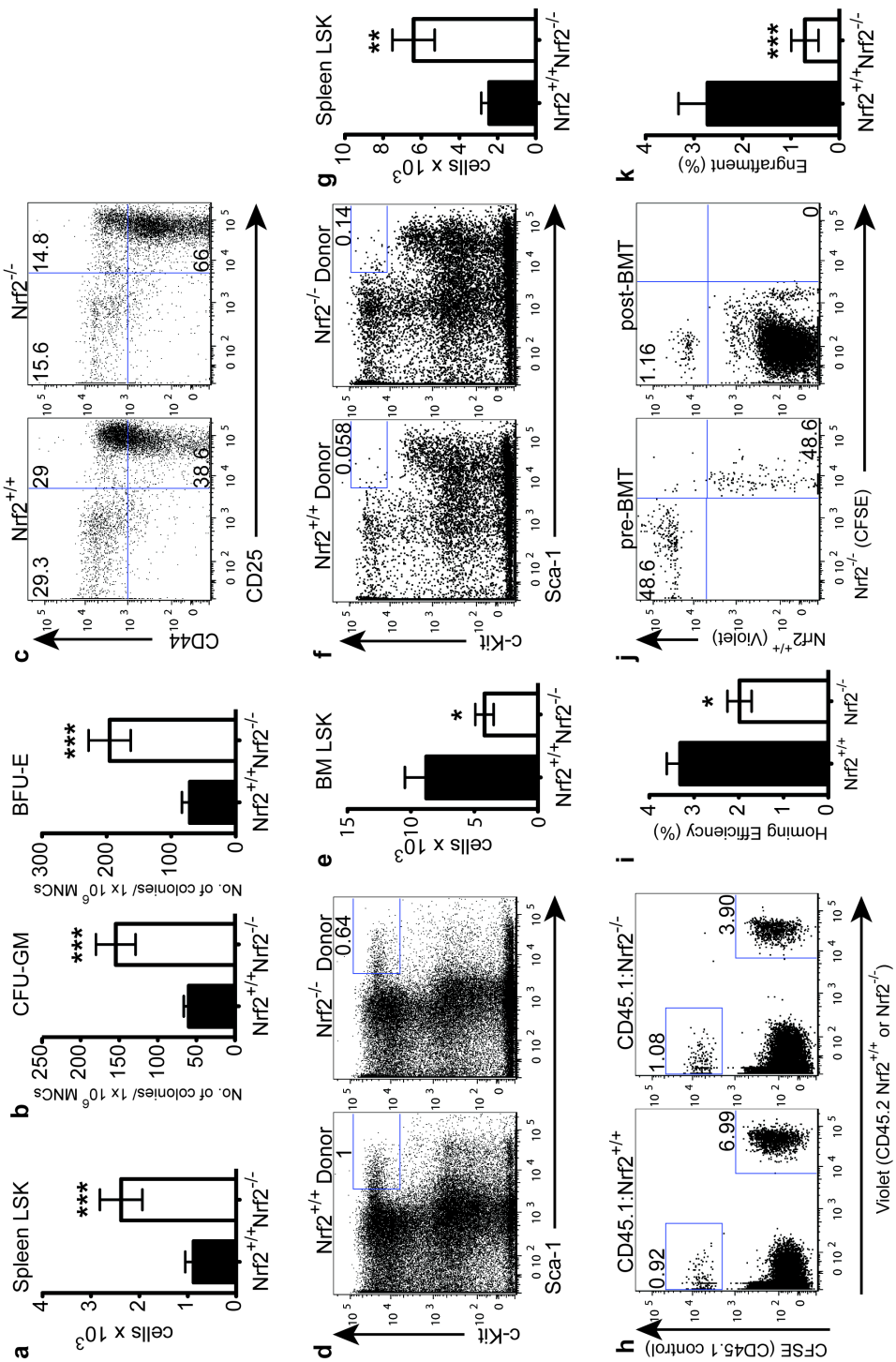

Nrf2 Mediates HSPC Function Through CXCR4

In addition to its well-described role as a crucial chemokine receptor for HSPC homing and retention, there has been considerable interest recently in the role of CXCR4 signalling for its role in maintaining HSC quiescence [18-20]. Strikingly, our findings on the role of Nrf2 on HSC homing and quiescence closely mirrored the observations in *Cxcr4*$^{-/-}$ adult animals. This directed us to investigate the interaction between Nrf2 and CXCR4. Although there was no change in the expression of VCAM-1 (**Figure 1.8, a, b**), another key molecule for HSPC homing, we found a 2-fold reduction in CXCR4 expression in *Nrf2*$^{-/-}$ LSKs compared to WT controls (**Figure 1.8, c, d**), which again was observed as early as in LT-HSC stage (**Figure 1.8, e, f**). This finding was functionally confirmed by performing *in vitro* transwell migration assays, where we found that *Nrf2*$^{-/-}$ LSKs migrated less efficiently towards CXCL12 at 6 hours (**Figure 1.8, g**), consistent with the reduced expression of CXCR4 caused by Nrf2-deficiency in HSPCs.

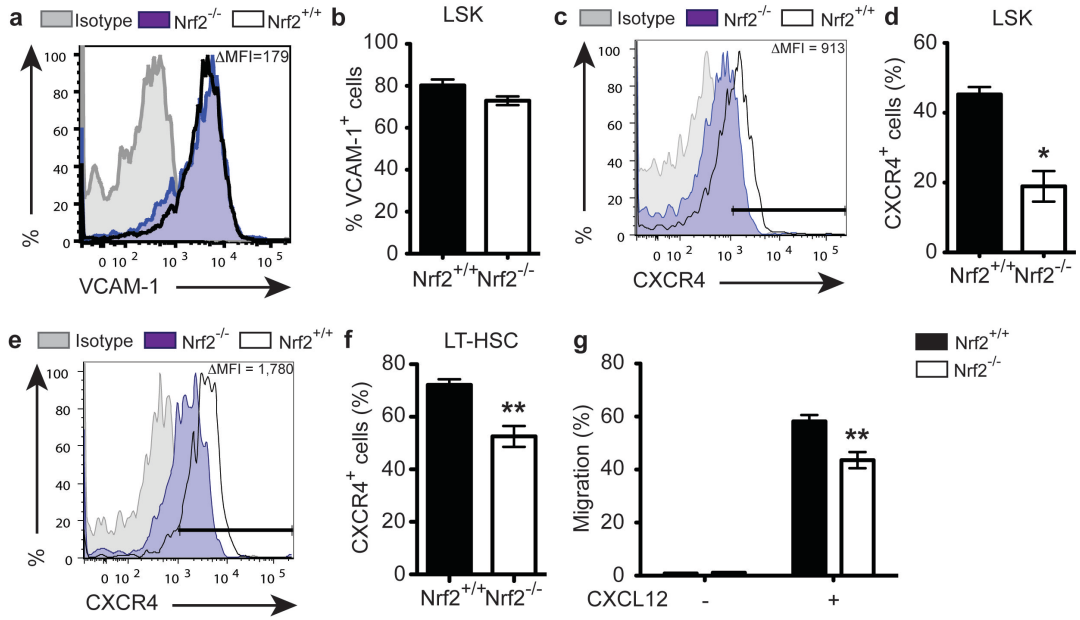

Figure 1.8. Reduced CXCR4 Expression in Nrf2$^{-/-}$ HSPCs

*(**a**) Representative flow cytometric analysis and (**b**) bar graphs showing the proportion of sorted WT and Nrf2$^{-/-}$ BM LSK cells expressing VCAM-1. Δ MFI (Mean fluorescence intensity) = (MFI of WT LSKs) - (MFI of Nrf2$^{-/-}$ LSKs). Data represent the mean ± SEM, n = 5 animals per strain. (**c**) Representative flow cytometric analysis and (**d**) bar graphs showing the proportion of sorted WT and Nrf2$^{-/-}$ BM LSK cells expressing CXCR4; mean ± SEM of 4 animals per strain. (**e**) Representative flow cytometric analysis and (**f**) bar graphs showing the proportion of sorted WT and Nrf2$^{-/-}$ BM LT-HSCs expressing CXCR4; mean ± SEM of 6 animals per strain. (**g**) Percentage of LSK cells that migrated toward unconditioned media with (+) or without (-) supplementation of CXCL12 at 6 hours of assays; mean ± SEM of 6 observations per strain over 2 independent experiments.*

To determine whether CXCR4 is a direct target of Nrf2, we scrutinised the promoter region of the mouse and human CXCR4 gene, and identified two putative conserved Nrf2 binding sites in the *Cxcr4* promoter (**Figure 1.9, a**). We cloned the *Cxcr4* promoter from mouse genomic DNA into a dual luciferase reporter vector, and demonstrated that exogenous Nrf2 transactivated the minimal promoter region *in vitro* (**Figure 1.9, b**). In addition, to assess whether endogenous Nrf2 binds to the *Cxcr4* promoter in BM, we conducted chromatin immunoprecipitation assays. We noted enrichment of both putative binding sites immunoprecipitated by Nrf2, confirming the physical interaction of endogenous Nrf2 and the *Cxcr4* promoter *in vivo* (**Figure 1.9, c**). Thus, Nrf2 directly binds to *Cxcr4* promoter and activates its expression.

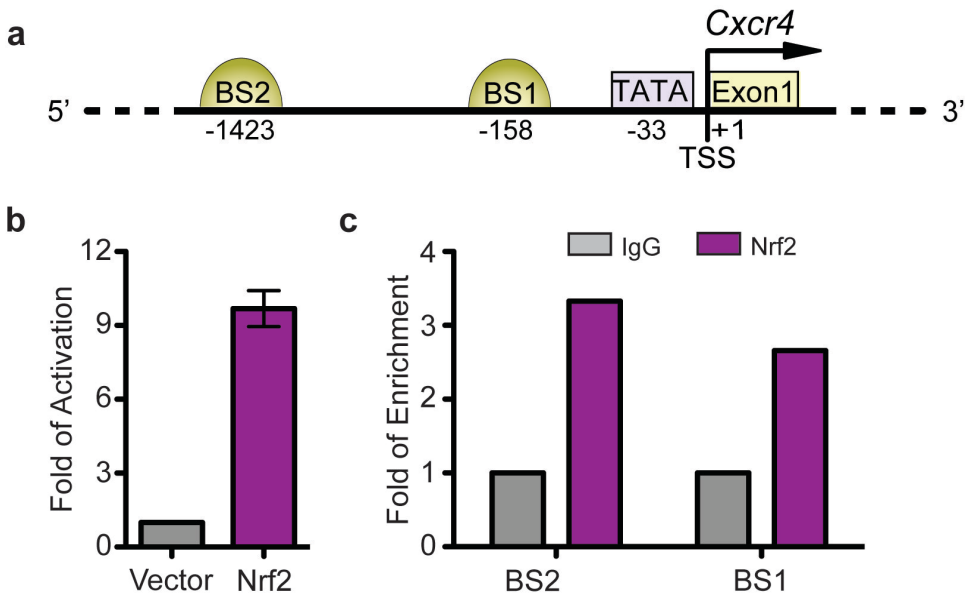

Figure 1.9. Nrf2 Regulates Cxcr4 Promoter

*(**a**) Schematic diagram representing the regulatory region of Cxcr4 promoter. The positions of potential transcription factor binding sites are noted (bp). BS, putative Nrf2 Binding Site; TSS, Transcription Start Site. (**b**) HEK293T cells were transfected with Cxcr4 promoter-driven luciferase reporter plasmids (covering -0.5 kb from TSS), and luciferase activity was assessed 24 hours after transfection. Data represent the mean ± SEM of 3 independent experiments. (**c**) Chromatin bound DNA from WT BM was immunoprecipitated with a Nrf2-specific antibody or IgG control. Quantitative PCR was performed using primers amplifying potential Nrf2 binding sites on Cxcr4 promoter. Data represent the mean of 2 independent experiments.*

Finally, we sought to examine whether dysregulation of CXCR4 expression contributed to the dual quiescence and migration defects observed in *Nrf2*$^{-/-}$ HSPCs. Lentiviral overexpression of CXCR4 in *Nrf2*$^{-/-}$ LSK cells restored the homing ability of *Nrf2*$^{-/-}$ HSPCs in transwell migration assays (**Figure 1.10, a, b**), as well as rescued the phenotype of *Nrf2*$^{-/-}$ HSPCs in their differentiation kinetics on OP9-DL1 co-culture to a comparable pace with WT LSKs (**Figure 1.10, a, c**). Taken together, these results suggest that Nrf2 controls multiple aspects of haematopoiesis at least partially through regulation of CXCR4 signalling.

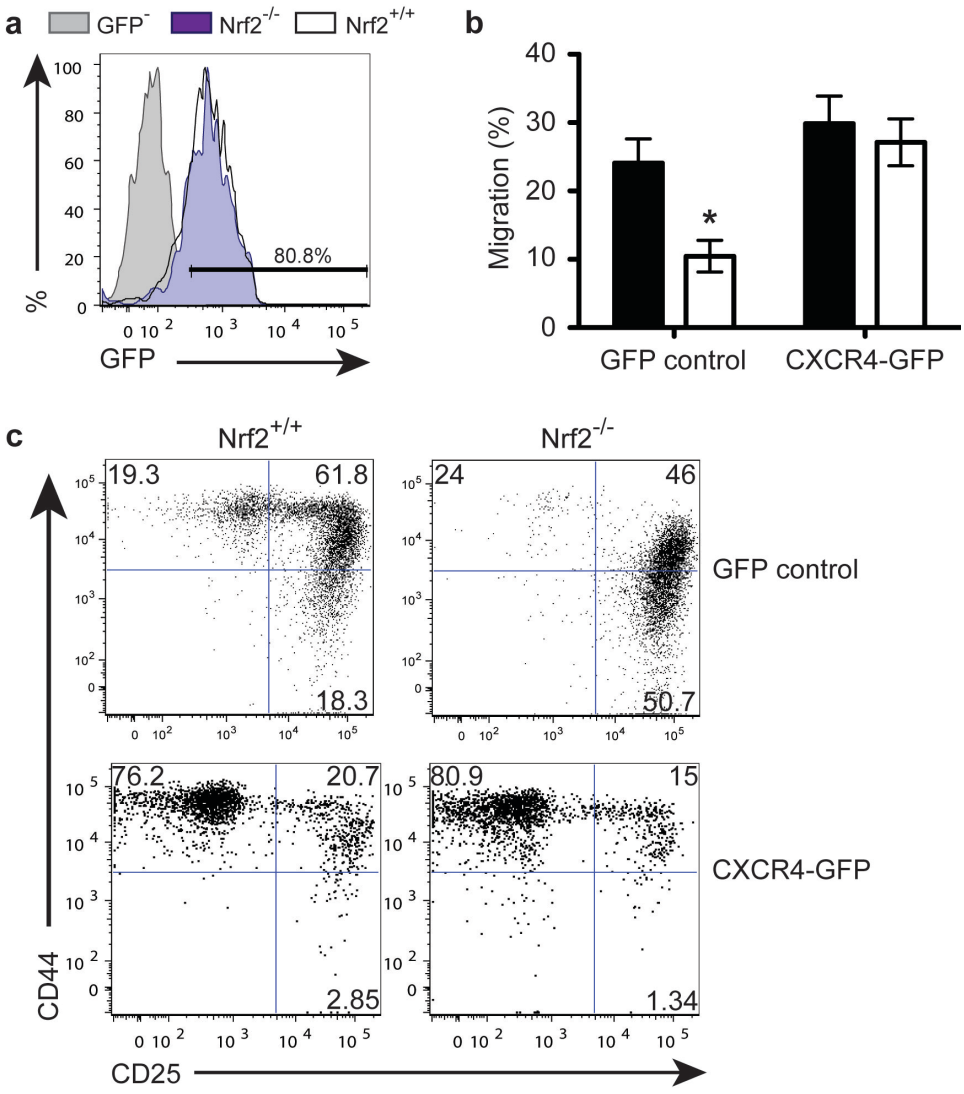

Figure 1.10. Nrf2 Mediates HSPC Functions Through CXCR4

*(**a**) Transduction efficiency of WT or Nrf2$^{-/-}$ LSKs with CXCR4-expressing vector (marked by expression of GFP) assessed 48 hours after transduction. (**b**) Percentage of GFP-transduced or CXCR4-overexpressing WT and Nrf2$^{-/-}$ LSK cells migrated toward unconditioned media supplemented with CXCL12 at 6 hours of assays; mean ± SEM of 5 independent experiments. (**c**) Representative flow cytometric analysis showing differentiation of WT or Nrf2$^{-/-}$ LSKs, transduced with GFP-control or CXCR4-overexpressing vector, at day 11 of OP9-DL1 co-culture, reproducible in 3 independent experiments.*

CHAPTER THREE

Nrf2 Regulates T-cell Alloreactivity

T cell activation promotes Nrf2 nuclear translocation and protein expression

To define the biological significance of Nrf2 in T-cell alloreactivity, we first assessed the expression pattern of Nrf2 in activated T cells. We found that total cellular Nrf2 expression in T cells was significantly increased 24 hours after T cell receptor (TCR) stimulation *in vitro* with α-CD3/CD28 (**Figure 2.1, a, b**). Moreover, there was approximately a 2-fold induction in the nuclear fraction of Nrf2 upon T cell activation (**Figure 2.1, a, c**). We questioned whether this increased nuclear translocation corresponds to enhanced transcriptional activities of Nrf2. Surprisingly, the expression of the canonical Nrf2 antioxidant target genes *Hmox1* and *Nqo1* was not increased in activated T cells (**Figure 2.1, d**), implying that additional, non-canonical, nuclear Nrf2 functions may exist upon TCR ligation. We next examined the effects of T cell allo-activation *in vivo* on Nrf2 activity. We used a well-established, fully MHC-mismatched murine allo-BMT model (B6 → BALB/c) for its potential for strong allo-activation and for its utility in subsequent GVHD studies. Compared to their syngeneic controls, donor-derived T cells, specifically the $CD4^+$ subsets, significantly upregulated their intracellular Nrf2 levels in the allogeneic setting (**Figure 2.1, e**). Taken together, these findings suggest a role for Nrf2 in T cell responses both *in vitro* and *in vivo*.

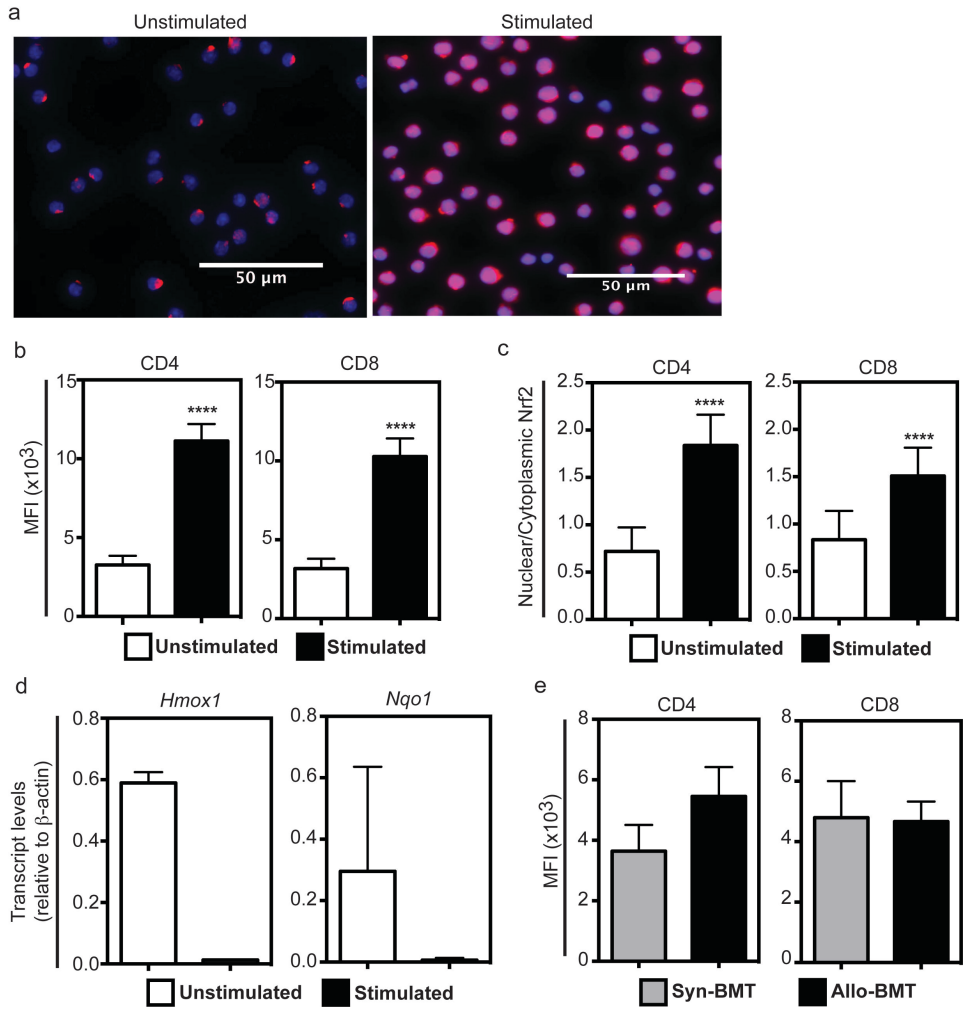

Figure 2.1. T Cell Activation Promotes Nrf2 Nuclear Translocation and Protein Expression

*Representative immunofluorescent images (**a**) and quantification of cellular mean fluoresecent intensity (MFI) (**b**) and nuclear:cytopalsmic ratio (**c**) of Nrf2 (purple) in T cells stimulated with a-CD3/CD28 for 24 hrs. The nucleus is defined by DAPI staining (blue). (**d**) Expression of Hmox1 and Nqo1 mRNA transcripts in T cells stimulated with a-CD3/CD28 for 24 hrs. (**e**) WT B6 T-cell depleted (TCD) BM and T cells were transplanted into lethally irradiated B6 (Syn-BMT) or BALB/c (Allo-BMT) recipients. Flow cytometric analysis on the intracellular levels of Nrf2 within donor T cells was performed using recipient spleens on Day 14 after BMT.*

Nrf2$^{-/-}$ donor T cells induces less GVHD mortality and morbidity

To specifically determine whether Nrf2 contributes to T-cell alloreactivity, we isolated *Nrf2*$^{-/-}$ splenic donor T cells and observed their ability to mediate acute GVHD in MHC-mismatched recipients (B6 → BALB/c). Importantly, wildetype (WT) and *Nrf2*$^{-/-}$ spleens displayed comparable total numbers and equally diverse TCR repertoire of both CD4^{+} and CD8^{+} T cell subsets under steady-state (**Figure 2.2, a, b**). Consistent with our hypothesis, MHC-mismatched recipients of *Nrf2*$^{-/-}$ donor T cells benefited from a significantly greater survival rate compared with recipients of WT T cells (**Figure 2.2, c**). Additionally, *Nrf2*$^{-/-}$ donor T cells led to significantly lower clinical GVHD scores and weight loss, resulting in an overall less GVHD morbidity in allo-BMT recipients (**Figure 2.2, d, e**). Moreover, these findings were recapitulated when a less fulminant, yet more clinically relevant, minor histocompatibility antigen (mHA)-mismatched model (B6 → LP) was used (**Figure 2.2, f - h**), indicating a critical role of Nrf2 in general rather than model-specific GVHD pathogenesis.

Figure 2.2. Nrf2*$^{-/-}$ *T Cells Induces Less GVHD Mortality and Morbidity

*(**a - b**) WT and Nrf2*$^{-/-}$ *splenocytes under steady-state were examined using flow cytometry for (**a**) T cell subset enumeration and (**b**) TCR Vb family repertoire. (**c - d**) Lethally irradiated BALB/c recipients received WT B6 TCD-BM alone, or with 0.5 x 10*^{6} *B6 WT or Nrf2*$^{-/-}$ *T cells were monitored daily for (**c**) survival and weekly for (**d**) GVHD clinical scores and (**e**) weight loss. (**f - h**) Lethally irradiated LP recipients received WT B6 TCD-BM alone, or with 2 x 10*^{6} *B6 WT or Nrf2*$^{-/-}$ *T cells were monitored daily for (**f**) survival and weekly for (**g**) GVHD clinical scores and (**h**) weight loss. Data represent the mean ± SEM.*

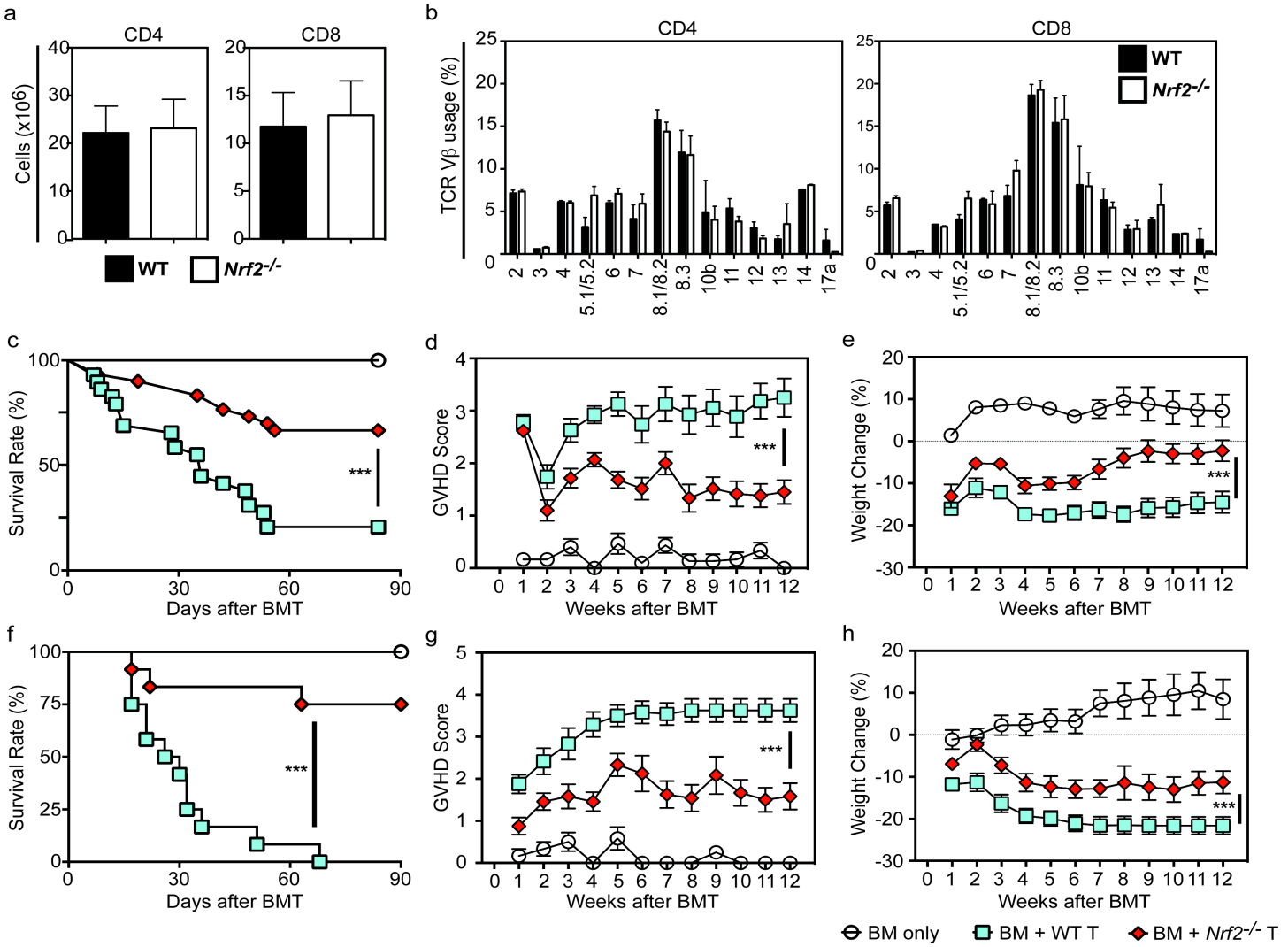
a
CD4
CD8
Cells (x10⁶)
WT
Nrf2-/-
b
CD4
CD8
TCR Vβ usage (%)
WT
Nrf2-/-
2
3
4
5.1/5.2
6
7
8.1/8.2
8.3
10b
11
12
13
14
17a
c
Survival Rate (%)
Days after BMT
***
d
GVHD Score
Weeks after BMT
***
e
Weight Change (%)
Weeks after BMT
***
f
Survival Rate (%)
Days after BMT
***
g
GVHD Score
Weeks after BMT
***
h
Weight Change (%)
Weeks after BMT
***
BM only
BM + WT T
BM + Nrf2-/- T

Nrf2 activity in allo-T cells contributes to hepatic, intestinal, and thymic GVHD

Acute GVHD results from activated donor allo-T cells recognizing alloantigens and destructing vital recipient organs, classically the triad of skin, liver, and gastrointestinal (GI) tract. While isolated skin GVHD does not contribute to mortality and the incidence of hepatic GVHD has become infrequent, GI GVHD has dominated the most severe and life-threatening cases following allo-BMT[21-23]. To determine whether the improved clinical outcomes of *Nrf2*$^{-/-}$ T-cell recipients could be attributed to reduced damage to specific GVHD target organs, we performed a semiquantitative histopathologic analysis of tissue samples in a blinded fashion after MHC-mismatched transplantation. In keeping with our hypothesis, recipients of *Nrf2*$^{-/-}$ T cells showed markedly reduced composite GVHD pathology scores, including liver, small bowel, and large bowel (**Figure 2.3, a**). Interestingly, however, Nrf2-deficiency in donor T cells did not significantly impact on the development of cutaneous GVHD, as indicated by the equivalent numbers of apoptotic keratinocytes in epidermis of WT and *Nrf2*$^{-/-}$ T-cell recipients (**Figure 2.3, b**). Additionally, donor allo-T cells mediate thymic GVHD, which leads to profound T cell deficiency and restricted repertoire following allo-BMT[24-27]. We discovered an increase in the overall thymic cellularity and the percentage of $CD4^{+}CD8^{+}$ double-positive (DP) thymocytes using flow cytometric analysis, reflecting significantly less thymic damage associated with GVHD, in the *Nrf2*$^{-/-}$ T cell recipients following allo-BMT (**Figure 2.3, c, d**). In short, these findings suggest that Nrf2 activity in donor T cells

contributes to the development of hepatic, GI, and thymic but not cutaneous GVHD.

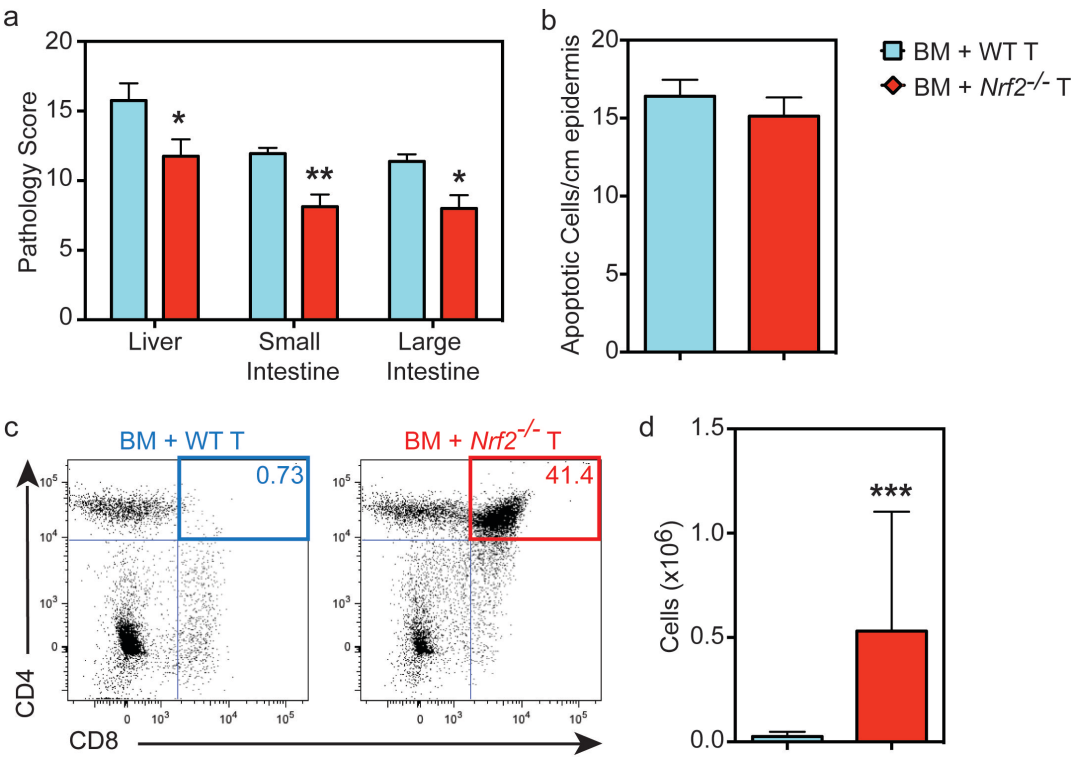

***Figure 2.3. Nrf2$^{-/-}$* Donor T Cells Results in Less Hepatic, Intestinal, and Thymic GVHD**

*Lethally irradiated BALB/c recipients received B6 WT TCD-BM and 0.5 x 10^6 B6 WT or Nrf2$^{-/-}$ T cells. GVHD target organs of recipients were analyzed on day 14. **(a)** H&E-stained slides of liver, small intestine, and large intestine were scored for histopathologic damage. **(b)** H&E-stained slides of skin were assessed for the number of apoptotc keratinocytes per cm of epidermis. **(c - d)** Flow cytometric analysis of thymic damage with **(c)** representative dot plots showing percentage and **(d)** enumeration of total $CD4^+CD8^+$ double-positive (DP) thymocytes.*

Nrf2$^{-/-}$ donor T cells display intact proliferation, activation, and apoptosis during the early phase of alloreactivity

Before infiltrating the target organs of recipients and as early as 12 hours following transfer, donor allo-T cells specifically trafficked to secondary lymphoid tissues where they undergo activation and proliferation upon exposure to alloantigen[28-31]. To assess whether the diminished GVHD activity of *Nrf2*$^{-/-}$ allo-T was due to defective early alloactivation, we transplanted CFSE-labeled T cells in MHC-mismatched recipients. In order to examine the extent to the proliferation of donor T cells that had undergone during alloactivation, we measured the rounds of CFSE dilution 96 hours following transfer using flow cytometry. Surprisingly, *Nrf2*$^{-/-}$ T cells displayed equivalent ability of alloantigen-induced proliferation, as indicated by the percentages of undivided and highly-proliferated fractions (CFSE^{low}) as well as the total numbers of highly-proliferated cells in recipient spleen (**Figure 2.4, a, b**). *Nrf2*$^{-/-}$ T cells also showed comparable activation, as determined by upregulation of CD25 and CD44 as well as downregulation of CD62L on the highly-proliferated alloactivated population (**Figure 2.4, d**). Additionally, T cells may undergo activation-induced cell death (AICD), a physiologically important process to control clonal expansion of activated T cells and contributes to downregulation of immune responses[32,33]. *Nrf2*$^{-/-}$ donor T cells demonstrated similar degree of apoptosis induced by alloactivation, as evidenced by the level of Annexin-V expression in highly-proliferated fractions (**Figure 2.4, c**).

Interestingly, although *Nrf2*$^{-/-}$ T cells showed equivalent proliferation and ACID during the initial alloactivation phase, we found a significantly greater number of *Nrf2*$^{-/-}$ CD8^{+} donor T cells in recipient spleens on days 7 and 14. Nonetheless,

these data suggest that proliferation, activation and apoptosis during the early phase of alloreactivity were unlikely to be contributory mechanisms for the better GVHD clinical outcomes induced by *Nrf2*$^{-/-}$ allo-T cells (**Figure 2.5, a**).

***Figure 2.4. Nrf2*$^{-/-}$ T Cells Display Intact Proliferation, Activation, and Survival**

Lethally irradiated BALB/c recipients were transplanted with 5 x 10^{6} *CFSE-labeled B6 WT or Nrf2*$^{-/-}$ *T cells. Recepient spleens were analyzed 96 hours after transplant by flow cytometry for CFSE dilution. (**a**) Comparable CFSE histogram overlays and (**b**) equivalent total numbers of CFSE*^{low} *WT versus Nrf2*$^{-/-}$ *donor T cells, gated on H-2Kb*$^{+}$ *events. (**c**) Similar expression of the apoptotic marker Annexin-V and (**d**) equivalent upregulation of the activation markers CD25, CD44 and downregulation of CD62L on WT versus Nrf2*$^{-/-}$ *donor allo-T cells, gated on H-2Kb*$^{+}$*CFSE*^{low} *populations.*

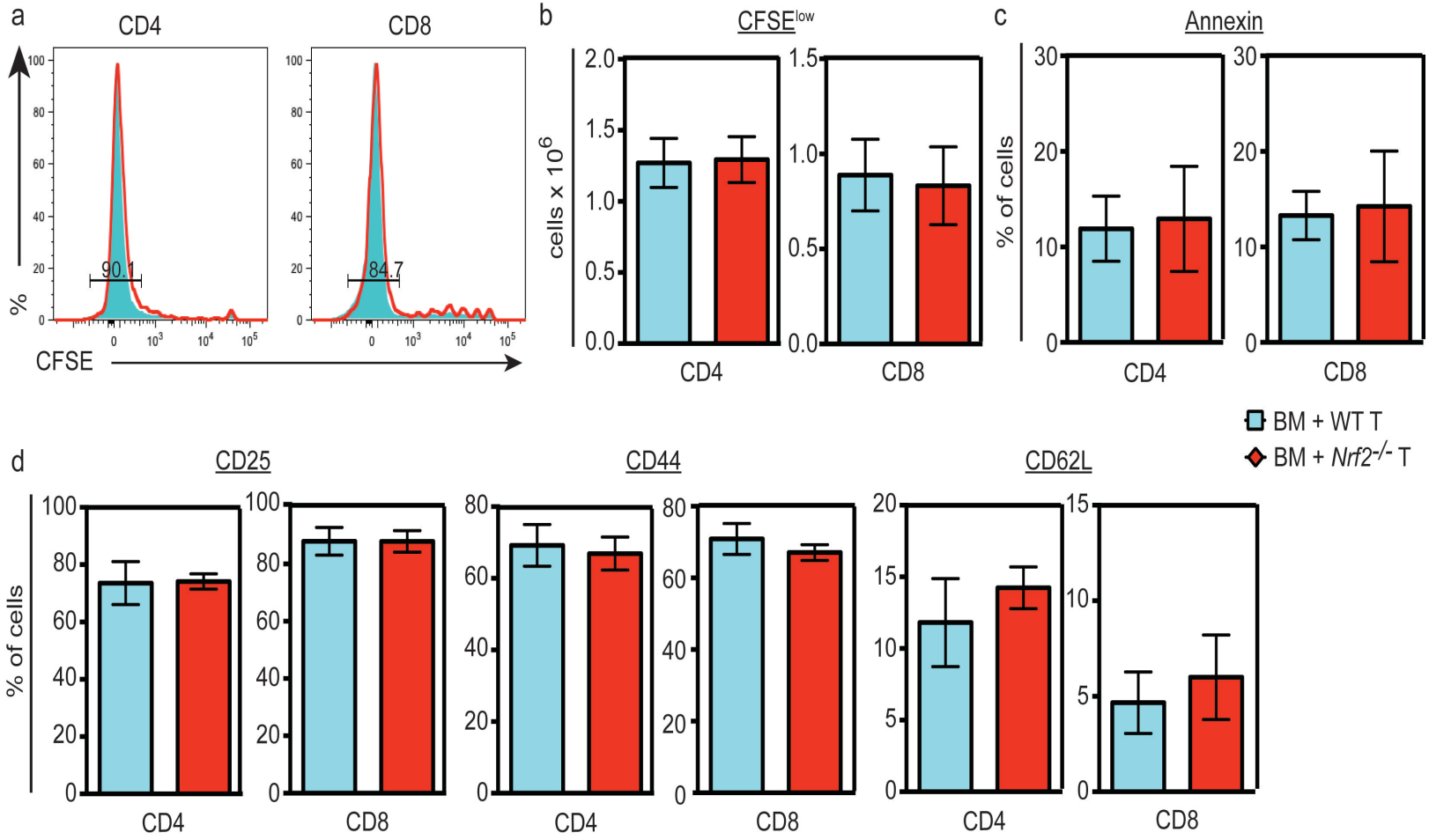
a
CD4
CD8
90.1
84.7
%
CFSE
b
CFSE^low
cells x 10^6
CD4
CD8
c
Annexin
% of cells
CD4
CD8
BM + WT T
BM + Nrf2^-/- T
d
CD25
CD44
CD62L
% of cells
CD4
CD8

Nrf2$^{-/-}$ donor T cells display decreased intestinal infiltration and LPAM-1 expression

While the levels of early activation and proliferation are comparable across all priming sites, different secondary lymphoid organs imprint distinct homing receptor phenotypes and thus specify the infiltration to GVHD target organs of evolving donor allo-T cells[30,34-39]. Specifically, antigen presenting cells (APCs) within mesenteric lymph nodes (MLNs) are known to play a pivotal role in upregulating gut-homing receptors on donor allo-T cells. Given the reduced hepatic and intestinal GVHD pathology observed in *Nrf2*$^{-/-}$ allo-T cell recipients, we questioned whether Nrf2 modulates allo-T cell trafficking to intestines. Importantly, we found equivalent numbers of donor T cells in recipient MLNs on days 7 and 14, indicating intact migration of *Nrf2*$^{-/-}$ donor T cells to secondary lymphoid organs (**Figure 2.5, b**). However, we observed defective trafficking of these cells into intestinal tissues, as demonstrated by a decrease in the lymphocytic infiltrate within the small intestine and the large intestine of *Nrf2*$^{-/-}$ allo-T cell recipients (**Figure 2.5, c**). We further examined the expression of gut-specific homing molecules of donor allo-T cells, including LPAM-1 (homing to small intestine, large intestine, and liver) and CCR9 (homing to small intestine). While we observed no difference in CCR9 expression, we saw a small but statistically significant decrease in the expression of LPAM-1 in *Nrf2*$^{-/-}$ donor CD8^{+} T cells in recipient spleens (**Figure 2.5, d, e**). Collectively, these data suggest that defective upregulation of LPAM by donor CD8^{+} T cells possibly underlies the attenuated GVHD severity caused by *Nrf2*$^{-/-}$ allo-T cells.

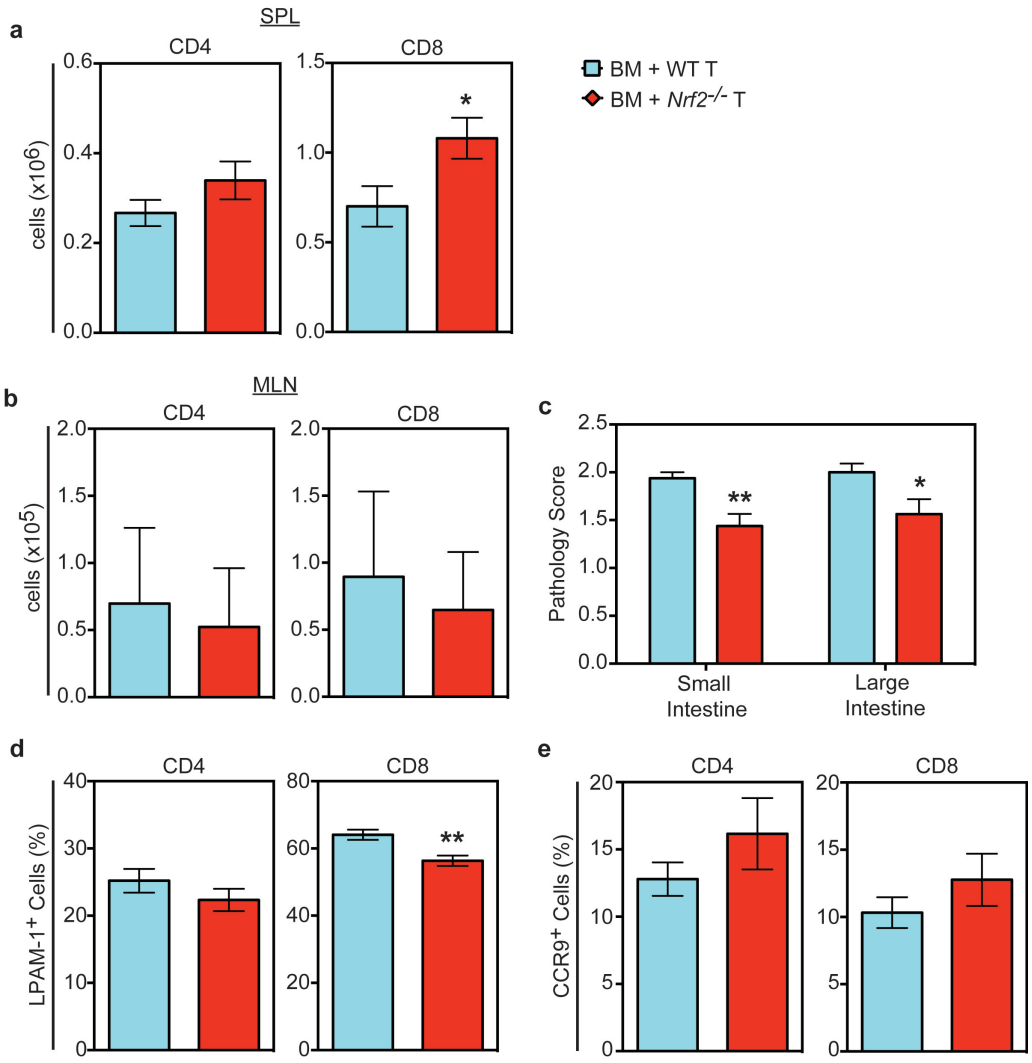

***Figure 2.5. Nrf2$^{-/-}$* Donor T Cells Display Decreased Intestinal Infiltration and LPAM-1 Expression**

*Lethally irradiated BALB/c recipients were transplanted with WT B6 TCD-BM and 0.5 x 10^6 B6 WT or Nrf2$^{-/-}$ T cells. Recipient organs were analyzed on day 14. (**a**) Spleens and (**b**) MLNs were analyzed for donor CD4 and CD8 T cells using flow cytometry. (**c**) H&E-stained slides of small and large intestines were scored for lymphocyte infitration. (**d – e**) Splenocytes were analyzed for the percentage of (**d**) LPAM-1 and (**e**) CCR9 expression in donor T cells.*

Abrogation of GVHD in *Nrf2*$^{-/-}$ allo-T cell recipients is associated with a greater proportion of donor-derived CD4^{+} Helios^{+} regulatory T cells

We next sought to evaluate the functional alterations of CD4^{+} allo-T cells as a result of Nrf2-deficiency. We proposed that Nrf2 may contribute to distinct compartmentalization in helper T helper cell (Th) subsets. Consistent with our hypothesis, analysis of intracellular levels of signature transcription factors required for different Th subsets revealed a significantly greater percentage and absolute number of donor-derived regulatory T cells (Tregs) in the spleen of *Nrf2*$^{-/-}$ allo-T cell recipient on day 7 post transplant (**Figure 2.6, a - c**). Tregs have been broadly defined into two main categories, thymus-derived natural Tregs (nTregs) and peripherally adapted induced Tregs (iTregs), both important in maintaining immune tolerance. To determine if Nrf2 regulates peripheral generation of iTregs, we activated naïve CD4^{+} T cells isolated from steady-state spleens under Treg differentiating cytokine conditions *in vitro*. Refuting our hypothesis, we observed an equivalent fraction of WT and *Nrf2*$^{-/-}$ CD4^{+} T cells polarized towards Tregs *in vitro* (**Figure 2.7, a, b**).

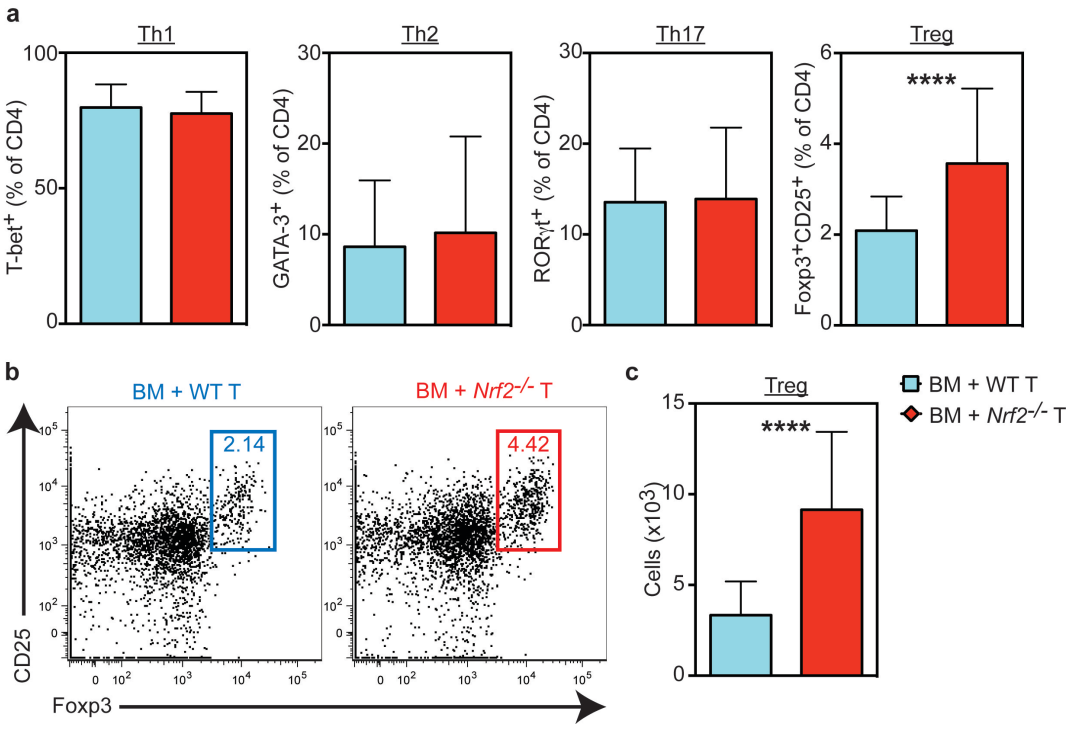

Figure 2.6. Nrf2 Ablation Alters Donor CD4$^+$ T Cell Compartmentalization

Lethally irradiated BALB/c recipients were transplanted with WT B6 TCD-BM and 0.5 x 10^6 B6 WT or Nrf2$^{-/-}$ T cells. Recipient spleens were stained for intracellular transcription factors for flow cytometric analysis of donor CD4$^+$ T cell subsets on day 7. ***(a)*** *Percentage of donor CD4$^+$ T cell subsets defined by the expression of T-bet (Th1), GATA-3 (Th2), RORgt (Th17) and Foxp3 with CD25 (Treg).* ***(b)*** *Representative flow cytometric dot plots showing the frequency of WT and Nrf2$^{-/-}$ donor Tregs within CD4$^+$ T cells.* ***(c)*** *Bar graphs showing absolute numbers of WT and Nrf2$^{-/-}$ donor Tregs.*

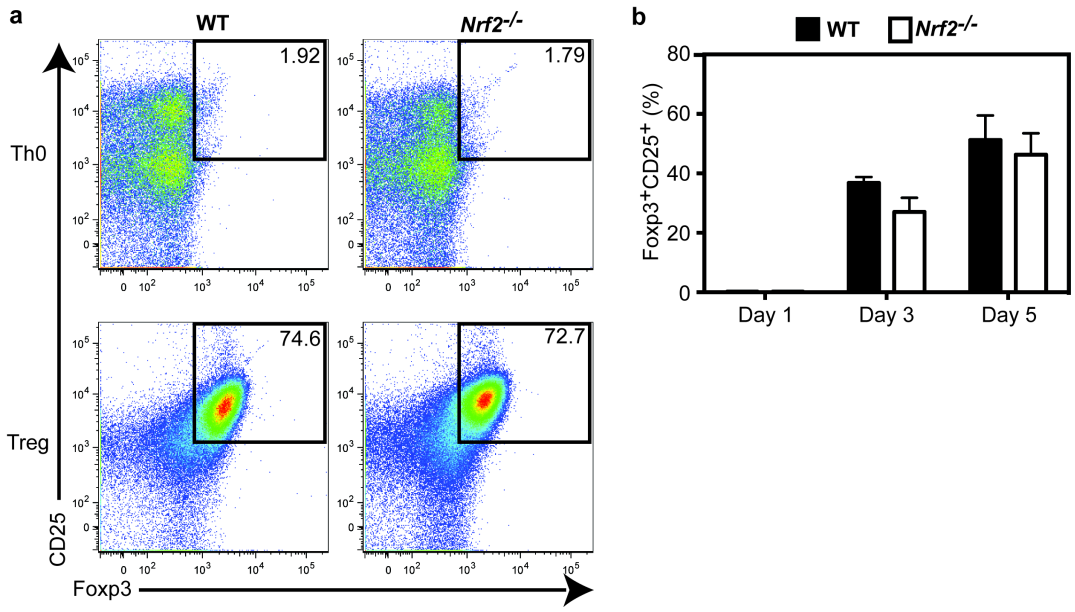

Figure 2.7. Nrf2 is Dispensible for Induction of Tregs in vitro

Naïve $CD4^+$ T cells isolated from steady-state WT or $Nrf2^{-/-}$ mice were cultured in non-polarizing (α-CD3/CD28 + IL-2) or Treg-inducing (+TGFb) conditions. ***(a)*** *Representative flow cytometric analysis showing percentage of induced Tregs on day 5.* ***(b)*** *Percentages of $CD4^+$ T cells polarized to Treg in Treg-inducing conditions on day 1, 3, and 5.*

It has been reported that the Ikaros transcription factor family member Helios and the membrane-bound tyrosine kinase receptor Neuropilin-1 (Nrp-1) are highly enriched in nTregs and thus their expression may serve as markers to discriminate nTregs from iTregs[40]. Interestingly, while we did not detect any differences in Nrp-1 expression (data not shown), we saw a significantly greater percentage of donor-derived Tregs expressing Helios in *Nrf2*$^{-/-}$ allo-T recipients on day 7 after BMT (**Figure 2.8, a, b**). Moreover, the amount of Helios expressed on a per cell basis was also significantly higher in donor *Nrf2*$^{-/-}$ Tregs compared to WT Tregs after allo-BMT (**Figure 2.8, a, b**). Notably, we did not observe any baseline differences in the total number or percentage of Tregs, and we found equally large fraction and high cellular expression of Helios within Treg populations in the donor inoculum prior to transplantation (**Figure 2.9, a - f**).

Additionally, recent literature suggests that Helios is required to stabilize the expression of the transcription factor FoxP3 and, thus by extension, the abundance and inhibitory activity of Treg cells in inflammatory settings[41,42]. In accordance with this notion, we identified an increase in the cellular FoxP3 protein expression within donor *Nrf2*$^{-/-}$ Tregs in the MHC-mismatched recipients, implying more stable suppression from *Nrf2*$^{-/-}$ Tregs on the alloreactive response[41] (**Figure 2.8, c, d**).

To further elucidate the biological significance of Nrf2 function on nTreg cells, we removed $CD4^{+}CD25^{+}$ putative Tregs from the donor inoculum and transplanted

only conventional T cells in MHC-mismatched recipients. We found that the survival advantage with *Nrf2*$^{-/-}$ allo-T cells during GVHD was completely abolished when Tregs were absent in the donor inoculum at the time of transplant (**Figure 2.8, e**). Taken these together, we conclude that Nrf2 function in donor T cells serves to undermine the stability of Tregs present in the graft during allo-BMT, most likely through downregulation of Helios expression of nTregs.

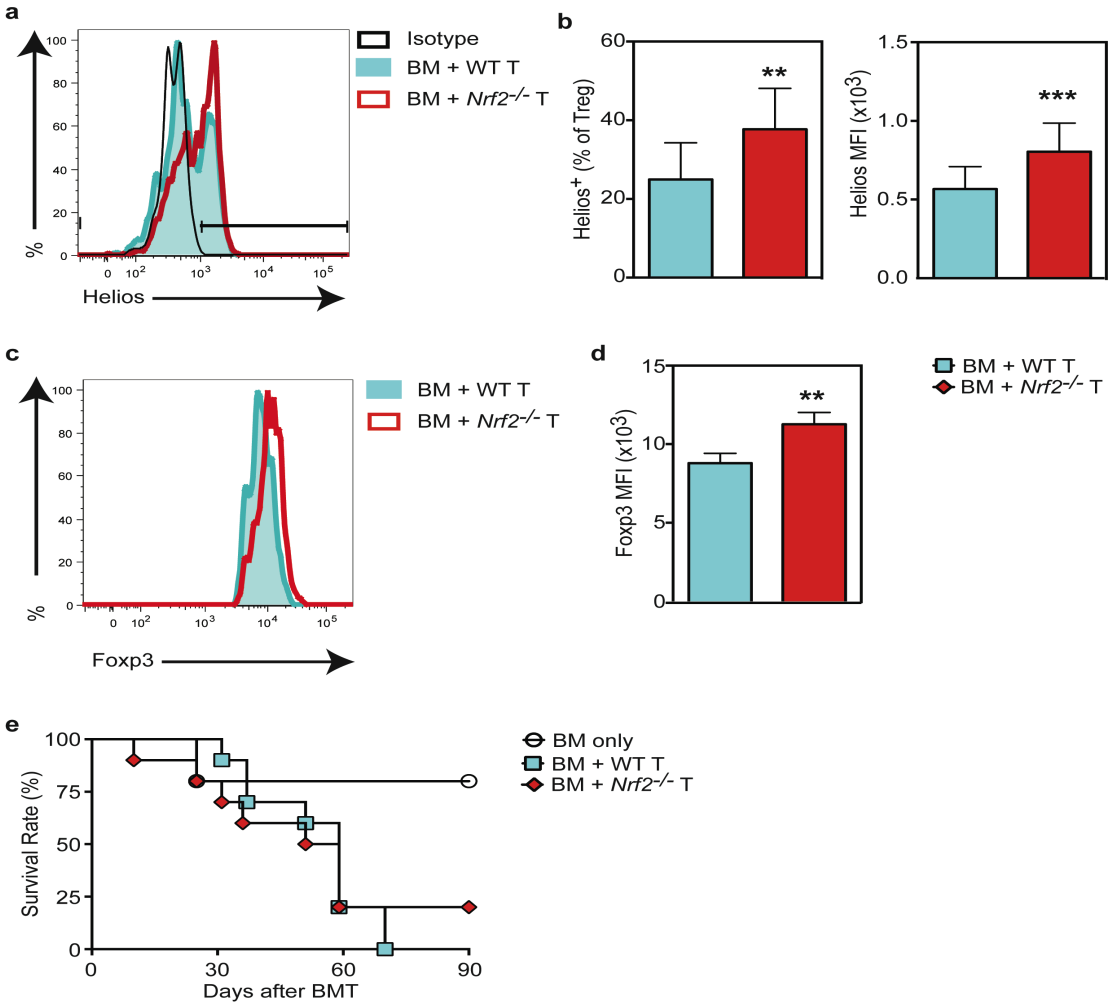

Figure 2.8. Abrogation of GVHD in Nrf2$^{-/-}$ allo-T cell recipients is associated with a greater proportion of donor-derived CD4^{+} Helios^{+} Tregs

*(**a** – **d**) Lethally irradiated BALB/c recipients were transplanted with WT B6 TCD-BM and 0.5 x 10^{6} B6 WT or Nrf2$^{-/-}$ T cells. Recipient spleens were analyzed on day 7 for intracellular expression of (**a, b**) Helios and (**c**, **d**) Foxp3 in donor-derived Tregs. (**e**) Lethally irradiated BALB/c recipients transplanted with WT B6 TCD-BM alone or with a total of 0.5 x 10^{6} Treg (CD4^{+}CD25^{+})-depleted B6 WT or Nrf2$^{-/-}$conventional CD4 and CD8 T cells (Tcon) were monitored daily for survival.*

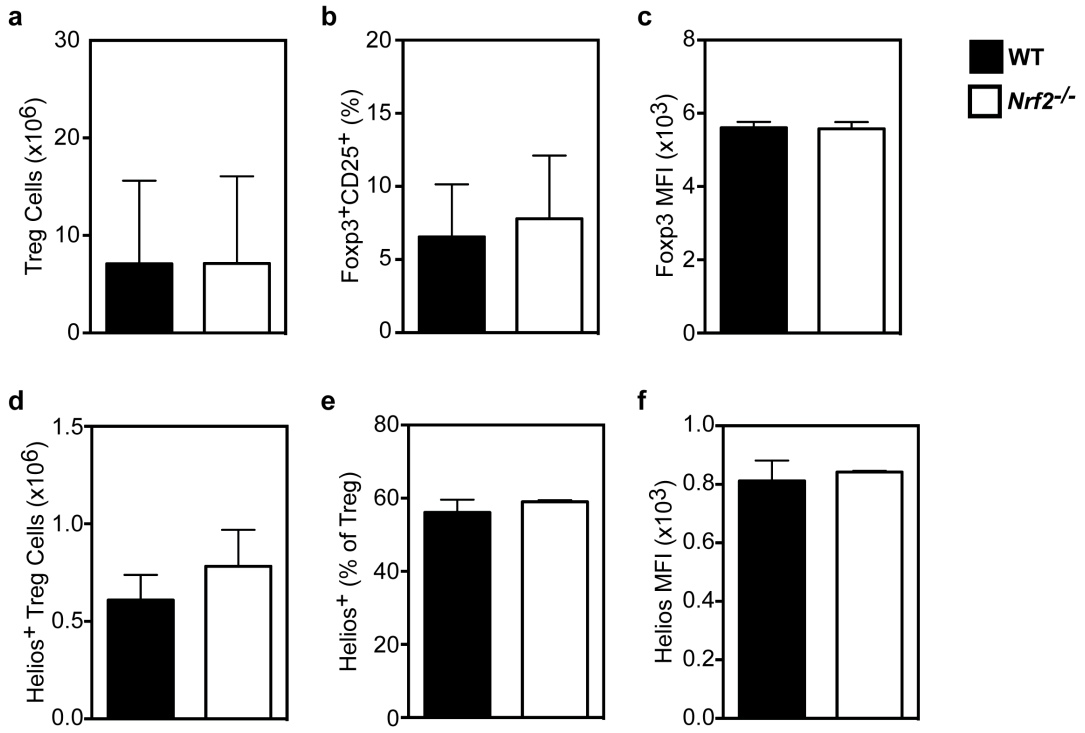

Figure 2.9. WT and Nrf2$^{-/-}$ Tregs under steady-state do not differ before transplantation

*WT and Nrf2$^{-/-}$ splenocytes under steady-state were examined using flow cytometry for (**a**) total number of Treg per spleen, (**b**) percentage of Treg within CD4^{+} T cells, (**c**) mean fluorescence intensity of Foxp3 within Treg, (**d**) total number of Helios+ Tregs (**e**) percentage of Tregs expressing Helios, and (**f**) mean fluorescence intensity of Helios within Treg.*

Nrf2$^{-/-}$ donor CD8^{+} T cell showed intact cytotoxicity and GVT capacity

We next sought to explore the role of Nrf2 on CD8^{+} T cell function independently from its effect on CD4^{+} T cells. To this end, we first activated naïve CD8^{+} T cells

isolated from steady-state spleens with TCR ligation *in vitro*, and examined their cytolytic capacity against a hematologic tumor bearing MHC-mismatched alloantigen (A20, murine B-cell lymphoma). *Nrf2*$^{-/-}$ CD8^{+} T cells displayed preserved specific killing ability *in vitro*, as measured by the comparable degree of chromium-51 (^{51}Cr) released from the pre-labeled tumor target cells after co-culture (**Figure 2.10, a**). To directly assess the cytotoxicity against alloantigen in an *in vivo* model as well as to maintain CD4^{+} help for CD8^{+} T-cell alloreactivity, we transplanted WT CD4 T cells mixed with WT or *Nrf2*$^{-/-}$ CD8^{+} T cells at a physiologic ratio (2:1) into MHC-mismatched recipients[43,44], which were subsequently challenged with fluorescently labeled allogeneic target cells mixed with control syngenic cells at 1:1 ratio on day 7 after allo-BMT[45,46] (**Figure 2.10, b**). Compared with BM only recipients, recipients of WT and *Nrf2*$^{-/-}$ CD8^{+} T cells demonstrated equally efficient elimination of allogenic targets, consistent with our *in vitro* findings (**Figure 2.10, a**).

Furthermore, to determine the clinical significance of preserved cytotoxicity of *Nrf2*$^{-/-}$ CD8^{+} T cells on GVHD pathogenesis, we followed the clinical course of MHC-mismatched allo-BMT recipients transplanted with WT CD4^{+} T cells mixed with WT or *Nrf2*$^{-/-}$ CD8^{+} T cells. As expected, WT and *Nrf2*$^{-/-}$ CD8^{+} allo-T cells resulted in equally high mortality when transplanted with WT CD4^{+} T cells (**Figure 2.10, c**). Importantly, we saw a significant reduction in mortality when *Nrf2*$^{-/-}$ CD4^{+} and WT CD8^{+} allo-T cells were transplanted, further supporting the notion that Nrf2 predominately regulates CD4^{+} and is dispensable for CD8^{+} T-cell alloreactivity.

Finally, we sought to determine the impact of Nrf2 deficiency on the GVT activity of allo-T cells in a well-established *in vivo* model: B6 → BALB/c with the A20 lymphoma cells. Using bioluminescent imaging (BLI), we were able to quantify tumor burden of established A20-TGL cell line that constitutively expresses firefly luciferase[47]. Compared with BM only recipients that rapidly developed tumor growth, recipients of *Nrf2*$^{-/-}$ T cells eradicated tumor as effectively as the WT T cells (**Figure 2.10, d, e**). With their diminished alloreactivity yet preserved tumor killing capability, *Nrf2*$^{-/-}$ T cells gave rise to an overall better survival in their allo-BMT recipients compared to WT T cells (**Figure 2.10, f**).

Figure 2.10. Nrf2 Is Dispensible for Donor CD8^{+} T-Cell Cytotoxicity and GVT Capacity

*(**a**) In vitro cytotoxicity assay. WT and Nrf2$^{-/-}$ CD8^{+} T cells isolated from steady-state spleens were pre-activated with α-CD3/CD28 in vitro for 72 hours followed by incubation with ^{51}Cr-labeled allogeneic A20 tumor target cells for 18-19 hours. (**b**) In vivo cytotoxicity assay. Lethally irradiated BALB/c recipients were transplanted with WT B6 TCD-BM and a total of 0.5 x 10^{6} T cells composed of B6 WT CD4^{+}T cells mixed with WT or Nrf2$^{-/-}$ CD8^{+} T cells at 2:1 ratio. On day 7, recipients were challegend with a 1:1 infusion of CFSE-labled BALB/c allogeniec and PKH26-labeled B6 syngeneic control targets, and elimination of targets was assessed in the spleen by flow cytometry 4 hours after challenge. (**c**) Lethally irradiated BALB/c recipients were transplanted with WT B6 TCD-BM alone or*

*with a total of 0.5 x 10^6 T cells composed of B6 WT vs Nrf2$^{-/-}$ CD4$^+$and CD8$^+$ T cells mixed at 2:1 ratio. Recipients were minitored daily for mortality. (**d - e**) Lethally irradiated BALB/c recipients transplanted with WT B6 TCD-BM alone or with 0.5 x 10^6 WT or Nrf2$^{-/-}$ T cells were challenged with 0.5 x 10^6 A20-TGL. The whole-body distribution of tumor burden was tracked weekly using bioluminescent signal intensity. (**d**) Representative bioluminescent images showing pseudocolor images superimposed on conventional phographs. (**e**) Tumor burden in mice quantified as biolominescent image flux. (**f**) Lethally irradiated BALB/c recipients transplanted with WT B6 TCD-BM alone or with 0.5 x 10^6 WT or Nrf2$^{-/-}$ T cells were challenged with 0.5 x 10^6 A20-TGL. Recipients were minitored daily for mortality.*

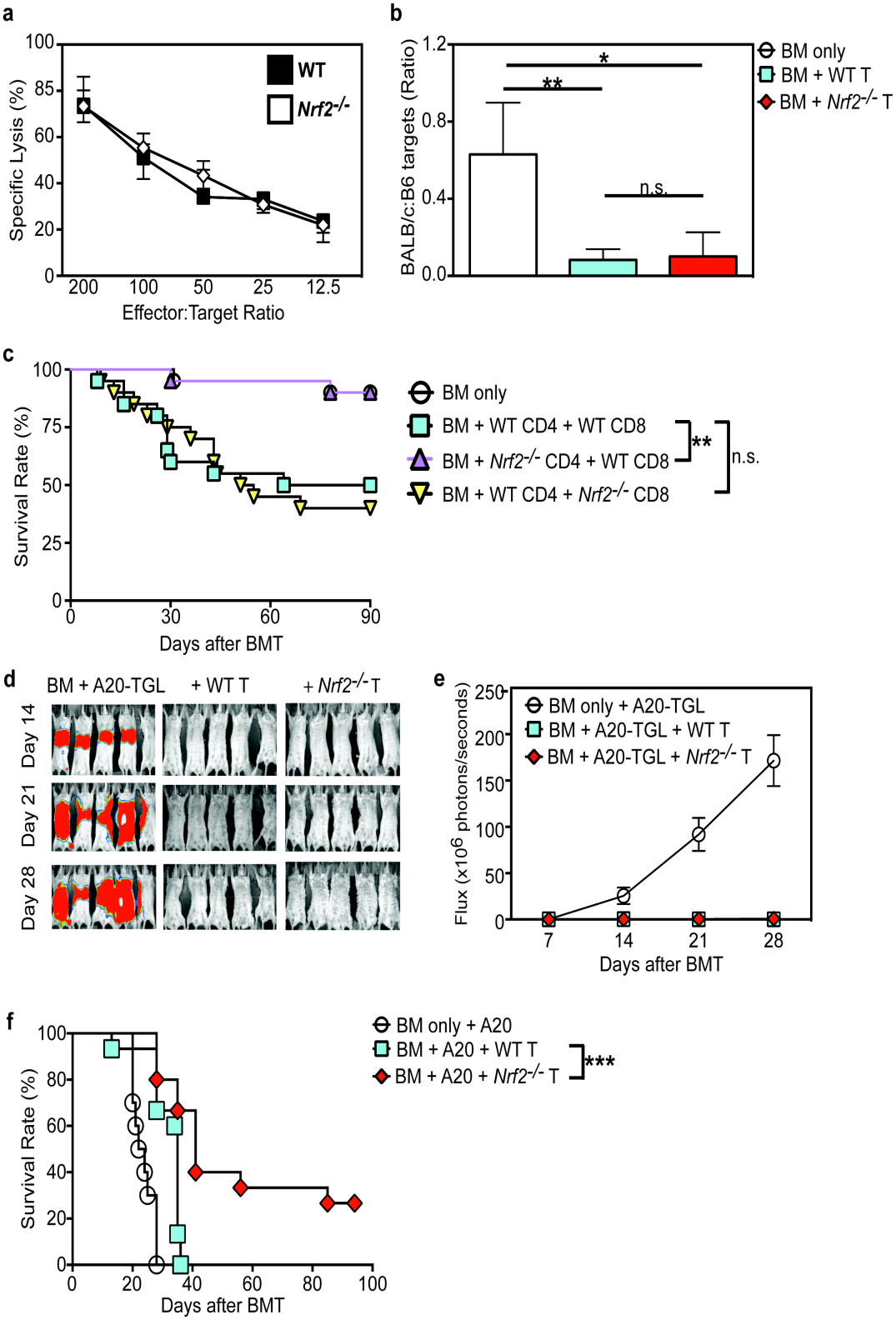
a
Specific Lysis (%)
Effector:Target Ratio
WT
Nrf2-/-
b
BALB/c:B6 targets (Ratio)
BM only
BM + WT T
BM + Nrf2-/- T
n.s.
c
Survival Rate (%)
Days after BMT
BM only
BM + WT CD4 + WT CD8
BM + Nrf2-/- CD4 + WT CD8
BM + WT CD4 + Nrf2-/- CD8
n.s.
d
BM + A20-TGL
+ WT T
+ Nrf2-/- T
Day 14
Day 21
Day 28
e
Flux (x10^6 photons/seconds)
BM only + A20-TGL
BM + A20-TGL + WT T
BM + A20-TGL + Nrf2-/- T
Days after BMT
f
Survival Rate (%)
Days after BMT
BM only + A20
BM + A20 + WT T
BM + A20 + Nrf2-/- T

CHAPTER FIVE

Discussion

Nrf2 Regulates HSC Function

Although Nrf2 has previously been reported to be dispensable for erythropoiesis and megakaryocyte differentiation [48-50], here we saw that it has a critical role in maintaining HSC function through its impacts on quiescence and self-renewal and, by extension, differentiation. Consistent with previous observations, we found that Nrf2 did not appear to control lineage specification, as *Nrf2*$^{-/-}$ HSPCs displayed typical myeloid and lymphoid commitment. Rather, our data argue that Nrf2 functions as a master regulator of the main modalities of HSC function. Not only do we show that Nrf2 can regulate the balance between quiescence and proliferation, but also between self-renewal and differentiation, as well as homing and retention of HSCs in the BM niche. This firmly establishes an important role for Nrf2 in the most primitive haematopoietic compartment. Moreover, our studies suggest that Nrf2 exerts its influence, at least in part, through direct regulation of CXCR4 expression. Importantly, previous studies have shown that among the cell cycle regulators investigated, cyclin D1 was singularly upregulated in *Cxcr4*$^{-/-}$ LSKs[20], consistent with our findings that cyclin D1 was upregulated in *Nrf2*$^{-/-}$ HSPCs.

There is increasing evidence that maintaining intracellular ROS at its basal level is necessary for HSC quiescence [51-55]. The most widely studied transcription factor

linking the ROS pathway to HSC quiescence and self-renewal are the FOXO (Forkhead O) proteins, which are important downstream effectors of the insulin/IGF-1 like signalling (ISS) pathway. Intriguingly, recent studies suggest that ISS not only inhibits DAF-16, the *C. elegans* homologue of FOXO, but also directly suppresses SKN-1, the *C. elegans* homologue of Nrf2, in aging [56]. There is also mounting evidence that the ISS and ROS signalling pathways cross-talk in the regulation of aging [57]. Interestingly, groups studying FOXO-deficient HSCs have found a similar phenotype to the one we describe here, alluding to the possibility that Nrf2 functions in parallel to the FOXO proteins as a downstream target of the PI3K-Akt pathway. Future research to validate the involvement of Nrf2 in the ISS pathway in mammalian models could be of considerable interest in understanding HSC aging [58].

Finally, a recent study has demonstrated a similar negative regulatory role for Nrf2 in intestinal stem cell proliferation [59]. Considering that Nrf2 is ubiquitously expressed, and stem cells and their progenitors are critical to the maintenance and function of various tissues, these findings indicate that Nrf2 serves as a master regulator of stem cell integrity and longevity in adult tissues. Future research into understanding and manipulating Nrf2 in tissue-specific stem cells and their niches may provide insights and innovative approaches to the field of regenerative medicine.

Nrf2 Regulates T-cell Alloreactivity

Allo-BMT represents a curative therapy for a variety of hematologic malignancies and can even contribute to the clearance of remnant malignancies through GVT reactions. Understanding and dissecting the undesired GVHD and beneficial GVT activities of allo-T cells is imperative for optimizing its therapeutic use by improving clinical outcomes of BMT recipients. In this study, we identified that Nrf2 within donor T cells contributes significantly to the GVHD activity, but is dispensable for GVT actions. In the absence of Nrf2 activation, acute GVHD is attenuated by the promotion of Helios^{+} nTregs, while GVT is preserved due to intact CD8^{+} cytotoxicity.

Nrf2 has been reported to modulate inflammation in different disease model, in which *Nrf2*$^{-/-}$ mice demonstrated increased susceptibility to experimentally induced sepsis, EAE, hepatitis, and asthma. However, it is clear that this is not its role in GVHD, as evidenced by our findings of reduced GVHD mortality, morbidity and pathology in the absence of Nrf2 activity. One possible explanation for the contrasting role of Nrf2 is the physiological differences among the models tested. Moreover, given the ubiquitous nature and thus the multiple potential targets of Nrf2, direct induction of inflammation in global *Nrf2*$^{-/-}$ mice may obscure the specific effects of Nrf2 activity in different cell subsets. Our study established the pro-inflammatory effects of Nrf2 signaling specifically within donor T cells by directly studying purified *Nrf2*$^{-/-}$ T cells in

a MHC-mismatched BMT model. Furthermore, the survival advantage seen in *Nrf2*$^{-/-}$ T cell recipients was even greater in a more clinically relevant mHA-mismatched model, further emphasizing the critical role of Nrf2 in T-cell alloreactivity and the clinical applicability of Nrf2 abrogation in the transplant setting.

Earlier studies specifically assessing the role of Nrf2 within T cells focused on the effects of Nrf2 activation in the cytokine production of CD4^{+} subsets *in vitro* and found conflicting results[14-16]. Yet a major limitation of these studies is the reliance of electrophilic compounds that target multiple pathways. Although the synthetic antioxidant tert-butylhydroquinone (tBHQ), for example, was commonly used to activate Nrf2 *in vitro* in these studies, it has also been reported to activate PI3K-Akt pathway and inhibit FoxO3a activity in other cell types[60-62]. One group observed an increase in Nrf2 expression as well as the transcripts of its classic antioxidant target genes when human T cells from healthy donors were activated *in vitro*[15]. However, this process seems to be independent from the oxidative stress, as the potent reducing agent N-acetylcysteine (NAC), known to prevent oxidative stress-dependent activation of Nrf2, failed to inhibit the induction of Nrf2 expression in activated T cells in the same study[15]. We similarly found an increased protein level and nuclear translocation of Nrf2, yet we did not observe an increase in its canonical antioxidant target genes in activated WT murine T cells *in vitro*. Nonetheless, these findings suggest a non-canonical Nrf2 pathway, either upstream and/or downstream, may exist during T cell activation. One

possible explanation is that the effects of Nrf2 activation on its canonical versus non-canonical targets are relative rather than absolute, and it may be dependent on TCR signal strength rather than oxidative stress.

Additionally, we demonstrated here that alloactivation *in vivo* enhanced intracellular level of Nrf2 in donor-T cells, namely within the $CD4^+$ subset, reiterating the biological significance of Nrf2 in $CD4^+$ T-cell alloreactivity. However, this upregulation of Nrf2 during allo-BMT is not required for initial alloactivation, since *Nrf2*$^{-/-}$ donor T cells displayed intact proliferation, activation and apoptosis during early phase of alloreactvity. Instead, Nrf2 exerts its effect during the expansion and target organ infiltration phase of acute GVHD, in which an increase in Tregs was seen in *Nrf2*$^{-/-}$ allo-T cell recipients on day 7 post transplantation. Furthermore, we demonstrated here that this increase in Treg was due to stabilization and/or increased expansion of nTregs present in the inoculum that were unleashed from Nrf2 and its proinflammatory property. This was evidenced by: 1) the disappearance of the survival advantage of *Nrf2*$^{-/-}$ allo-T recipients when putative Treg was removed from the graft before transplant; and (2) the relative increase in Helios expression, a marker for nTreg and critical for FoxP3 stability, in donor-derived *Nrf2*$^{-/-}$ Tregs only after but not before transplant. This augmentation in Treg in the absence of Nrf2, whether preceding or following it, is associated with reduced systemic inflammation after allo-BMT, as shown by the ameliorated GVHD-induced hepatic, intestinal, and thymic damage in *Nrf2*$^{-/-}$ donor T cell recipients.

Critical for their potential translation into improved allo-BMT strategies, *Nrf2*$^{-/-}$ donor T cells retained their GVT ability against hematologic malignancies. We demonstrated here that *Nrf2*$^{-/-}$ donor CD8^{+} T preserved high quality of killing and antitumor activity, and a greater quantity of CD8^{+} counts accumulating in the spleen of *Nrf2*$^{-/-}$ allo-T cell recipients. One likely contributory mechanism is the defective upregulation of LPAM-1 in *Nrf2*$^{-/-}$ CD8 T cells, possibly secondary to suppression from increased nTregs on APC priming, restrained them from infiltrating and damaging GVHD target organs and trapped them in the secondary lymphoid organs where lymphohematopoietic tumor cells like A20 resides. *Nrf2*$^{-/-}$ donor CD8^{+} T cells also possess a higher homeostatic proliferative potential under lymphopenic environement (data not shown), further contributing to increased circulating *Nrf2*$^{-/-}$ donor CD8^{+} T cells fully capable of combating liquid cancer. Moreover, our group has previously shown that, T cells lacking functional LPAM-1 receptors as a result of β7 subunit deficiency actually have enhanced tumor clearance ability while causing less acute GVHD in their MHC-mismatched recipients[63,64]. Furthermore, donor Tregs have previously been reported to be dispensable for GVT activity while inhibiting GVHD after allo-BMT[44]. It is also important to remember that, in addition to GVHD suppression, donor Tregs (also CD8) have previously been shown to promote hematopoetic stem and progenitor cells (HSPC) engraftment as well as enhance immune reconstitution[65,66]. Last but not the least, mounting evidence suggests that Nrf2 confers proliferation, survival and chemoresistance in various tumors including hematologic cancers[9,11,12]. Collectively, these findings support for

developing new therapies directed toward the Nrf2 pathway as an antitumor adjuvant and a strategy to prevent GVHD in patients undergoing allo-BMT.

In the second part of the dissertation, we show for the first time a comprehensive analysis of the role of Nrf2 in T cell function *in vivo*. We present here that inhibition of Nrf2 activity in donor T cells ameliorates GVHD severity without compromising GVT activity. Our findings not only shed light on the biological significance of Nrf2 in T-cells as well as the fundamental immunological differences between GVHD and GVT actions, but also potentially reveal exciting therapeutic targets for treating patients with hematologic malignancies and GVHD.

CHAPTER SIX

Materials and methods

Mice

Nrf2$^{-/-}$ mice were a kind gift from Dr. Jefferson Chan (University of California, Irvine), and were backcrossed to C57BL/6 background for 7-8 generations. Wild-type (*Nrf2*$^{+/+}$) C57BL/6 (CD45.2) or B6.SJL-*Ptprc*^{a}*Pepc*^{b}/BoyJ (CD45.1) mice were purchased from the Jackson Laboratory (Bar Harbor, ME). All mice were age-matched, female *Nrf2*$^{+/+}$ and *Nrf2*$^{-/-}$ mice (8 to 12 weeks old). All mice were maintained in the MSKCC Animal Facility in Thorensten units with filtered germ-free air. Experiments were conducted in compliance with institutional guidelines at MSKCC.

Cell Isolation

BM cells were flushed from intact femurs and tibia, and spleens were mashed with glass slides to generate single cell suspension. Collection of the cells was performed in RPMI media with 10% FBS or PBS with 0.5% BSA, and filtered through a 70-μm strainer. Unless otherwise stated, all cell numbers in this study were standardized as total counts per leg or per spleen.

Flow Cytometry

Monoclonal antibodies (mAbs) recognizing the following markers were used for flow cytometric analyses and cell sorting (LSR II or FACSAria III, BD Biosciences, NJ): (from BD Pharmingen, NJ) c-kit (2B8), Sca-1 (D7), CD11b (M1/70), CD11c (HL3), CD19 (ID3), CD3ε (145-2C11), CD34 (RAM34), CD4 (RM4-5), CD45 (30-F11), CD45.1 (A20), CD45.2 (104), CD48 (HM48-1), CD8α (53-6.7), CD62L (MEL-14), CD135 (A2F10.1), Gr-1 (RB6-8C5), NK1.1 (PK136), TER-119 (TER-119), CXCR4 (2B11), VCAM-1 (429), Rat $IgG_{2a}\kappa$ isotype (B39-4); (from eBioscience, CA) CD127 (A7R34), CD150 (mShad150), CD16/CD32 (93); (from Invitrogen, CA) B220 (RA3-6B2), and streptavidin (N/A). The lineage antibody cocktail included anti-CD3, anti-CD4, anti-CD8α, anti-CD19, anti-CD11b, anti-CD11c, anti-Gr-1, anti-NK1.1, and anti-TER119. Nuclear staining of Ki-67 was done using anti-human Ki-67 antibody (MOPC-21) (BD Pharmingen, NJ) and fixation/permeabilisation solutions (eBiosciences, CA).

Colony-Forming Cell Assays

BM cells (5×10^4) or splenocytes (1×10^5) were plated in triplicate in 35-mm tissue culture dishes (Nalge Nunc, NY) containing 1 mL assay medium consisting of IMDM, 1.2% methylcellulose (Fisher Scientific, NJ), 30% FBS, 5×10^{-5} M 2-mercaptoethanol, 2 mM L-glutamine, and 0.5 mM hemin, and supplemented with rmSCF (20 ng/mL), rmIL-3 (20 ng/mL), and human erythropoietin (EPO, 6 U/mL) (Amgen Inc, CA). After 10 days of incubation at 37°C in 5% CO_2 in air, CFU-GM, BFU-E, and CFU-Mix were scored under an inverted microscope.

Cobblestone Area Forming Cell Assay

MS-5 cells were seeded in 12.5 cm^2 tissue culture flasks in α-MEM with 10% FBS. When the cells reached confluence, medium was replaced with long-term culture (LTC) medium: MEM-α, 12.5% FBS, 12.5% horse serum (HyClone Lab. Inc., UT), 10^{-6} M hydrocortisone (Sigma Chemical Co., MO) and 5×10^{-5} M 2-mercaptoethanol. BM cells (5×10^5) or Lin^- splenocytes (1.5×10^4) were added per flask in triplicates. The cultures were demidepopulated weekly and fed with fresh LTC medium. After 3 weeks of culture, CAFCs were scored as phase-dark hematopoietic clones of at least 5 cells beneath the stromal layer using an inverted microscope. After scoring CAFCs at week 3, suspension cells and adherent cells that were detached by treatment with 0.05% trypsin/0.53 mM EDTA were assayed in methylcellulose for CFU-GM or replated in fresh MS-5 cells for secondary CAFC assay. The co-cultures of secondary CAFC assay were again scored at week 3.

Cell Culture

Co-culture of HSPCs and OP9-DL1 stromal cell lines was previously described [67]. Briefly, isolated LSK cells were seeded on a 60-80% confluent monolayer of OP9-DL1 cells into six-well tissue culture plates in α-MEM, supplemented with 20% FBS, 100U/mL of penicillin, 100μg/mL of streptomycin, 5ng/mL of rmIL-7 (Miltenyi Biotec, CA), and rm5ng/mL of Flt3L (Miltenyi Biotec, CA). Cells were maintained at 37°C in a humidified atmosphere containing 5% CO_2, and were collected at indicated intervals.

Bone Marrow Transplant

In the serial transplantation assay, we purified BM LSK cells from CD45.2^{+} (WT or *Nrf2*$^{-/-}$) donors and CD45.1^{+} (WT) competitors, mixed them at 1:1 ratio, and transplanted 2 × 10^{3} cells into lethally irradiated CD45.1^{+} (WT) mice (1,100 cGy total body irradiation, split dose) via tail vein injection. After 4 months of reconstitution, we assessed chimerism of donor-derived LSK cells (CD45.2^{+}) in the recipient BM, as well as sort purified these cells, mixed them with new CD45.1^{+} (WT) competitors at 1:1 ratio, and transplanted them into a second set of lethally irradiated CD45.1^{+} (WT) mice. Chimerism in the BM was again assessed 4 months after secondary transplant. In the chimeric repopulation study, we isolated LSK cells from donor BM and transplanted 2 × 10^{3} cells into lethally irradiated mice, and analysed reconstitution in BM after 8 weeks. In the *in vivo* homing assays, we isolated Lin^{-} BM cells from CD45.1^{+} (WT) and CD45.2^{+} (WT or *Nrf2*$^{-/-}$) donors using a lineage cell depletion kit (Miltenyi Biotec, CA) per manufacturer's instructions. We labelled the isolated cells with 5μM CellTrace^{TM} Violet Cell Proliferation Kit for flow cytometry (Invitrogen, CA) or CFSE (Invitrogen, CA) per manufacturer's recommendation, mixed the labelled CD45.1^{+} and CD45.2^{+} Lin^{-} BM cells at 1:1 ratio, then transplanted 2 × 10^{6} cells into lethally irradiated recipients for analysis 18 hours post-transplant. We also isolated WBM cells from CD45.2^{+} WT and *Nrf2*$^{-/-}$ donors, labelled them with CellTrace^{TM} Violet Cell Proliferation Kit and CFSE respectively, mixed them at 1:1 ratio, then transplanted 16 × 10^{6} cells into lethally irradiated recipients for analysis of LT-HSC engraftment 16 hours following the transplant.

Cell Cycle Analysis

Purified BM cells (LSKs or LT-HSCs) were fixed with ice-cold 4% paraformaldehyde at 4^{o}C overnight, washed with PBS twice, then labeled with 20μg/mL Hoechst 33342 (Invitrogen, CA) and 1μg/mL pyronin Y (Sigma-Aldrich, MO) for 20 minutes before flow cytometric analysis.

Immunohistochemistry

Fresh tibiae were collected and fixed in 10% formalin at room temperature overnight, decalcified for 24 hours using Decalcifier I (Surgipath, IL), washed with water, and embedded in wax. 5 μm paraffin sections were prepared using a microtome (Leica Microsystems, Germany). The sections were dewaxed in xylene, hydrated in graded alcohols, blocked in 1% hydrogen peroxide, and treated in pH6.0 10mM citrate buffer. The sections were then incubated with primary antibody Cyclin D1 (Thermo Scientific, MA) overnight, followed by appropriate secondary antibodies and avidin-biotin complexes (Vector Laboratories, CA). Antibody reaction was visualized with 3-3' Diaminobenzidine (Sigma-Aldrich, MO) and counterstained with haematoxylin. Tissue sections were dehydrated in graded alcohols, cleared in xylene and mounted.

5-FU Treatment

5-FU (InvivoGen, CA) was administered to mice intraperitoneally at a dose of 150mg/kg either as a single dose or once every 7 days consecutively for 3 times. BM cellularity was examined at day 3.5 in the former experiment, and the survival of individual mice was monitored daily in the latter.

Transwell Cell Migration Assay

Purified LSK cells were incubated in IMDM media containing 20% FBS, 20ng/mL murine IL-3 (PeproTech Inc., NJ), 20ng/mL SCF (PeproTech Inc., NJ), and 20ng/mL Flt3L (Amgen Inc., CA) 37^{o}C in a humidified atmosphere containing 5% CO_2 for 18 hours. LSK cells were then washed with IMEM media twice, resuspended in QBSF media (Quality Biologicals Onc., MD) in 0.1 × 10^6/mL. 100μL of cell suspension was loaded to the upper chamber of the transwell, and 600μL of QBSF media with or without CXCL12 (200ng/mL, R&D systems, MN) was added to the lower chamber of the transwell plate (pore size 5μm, Corning, NY). Cells were allowed to migrate across the membrane at 37^{o}C with 5% CO_2 incubator, and their migration efficiency was assessed at 6 hours.

Luciferase Reporter Assay

CXCR4 promoter regions were identified within 2kb upstream from the transcription start site of mouse CXCR4 sequence (Genebank accession number NC_000067) as previously described[68]. Putative Nrf2 binding sites were predicted using PROMO (http://www.lsi.upc.es/~alggen). 500bp upstream from transcription start site of mouse CXCR4 was amplified by PCR from WT C57BL/6 mouse genomic DNA and subsequently subcloned into the pGL4.23 luciferase reporter vector (Promega, WI), and named pCXCR4. pCXCR4 construct was co-transfected into HEK293T cells using lipid-based 293T TransIT Reagent (Mirus Bio, WI) with either pUC19 empty vector or Nrf2- pCMV vector, as well as phRL-TK vector as an internal control. Cells were collected 24 hours after

transfection and both luciferase activity was determined using Dual-Luciferase Reporter Assay System (Promega, WI) as per manufacturer's instructions.

Chromatin Immunoprecipitation Assay (ChIP)

ChIP assays were performed using the ChIP Assay Kit (Upstate Biotechnology, EMD Millipore, MA) as per manufacturer's instruction. Mouse WBM cells were used to assess the binding of Nrf2 to potential binding sites in *Cxcr4* promoter. Chromatin was incubated with normal mouse IgG or an anti-Nrf2 antibody (C-20) (Santa Cruz, CA). Input and immunoprecipitated DNA were analyzed by quantitative PCR with primer pairs spanning the Nrf2 binding sites identified in the *Cxcr4* promoter (TBS2: AACCGAAAGCCTTCCTTAGC and TGATGATCCCGTTTGTCACC; TBS3: ATCCACGTGGGTAAGGATGG and AGAAGTCCAAGAGCCACTGC).

Lentiviral Transduction

CXCR4 cDNA from pORF-mCXCR4 plasmid (Invivogen, CA) was subcloned into a plasmid encoding recombinant lentiviral vector with eGFP reporter (a kind gift from Dr. Michel Sadelain). Viral particles were produced in HEK293T cells using lipid-based 293T TransIT Reagent (Mirus Bio, WI) as previously described[31]. Freshly purified LSK cells were resuspended in 0.2×10^6/mL of QBSF media (Quality Biologicals Onc., MD), supplemented with 10ng/mL rmSCF (Miltenyi Biotec, CA), 20ng/mL rhIGF-2 (Miltenyi Biotec, CA), 10ng/mL rhFGF II (Miltenyi Biotec, CA), 100ng/mL rhTPO (Miltenyi Biotec, CA). Concentrated

viral particles were added to cell suspension with 0.8 μg/mL polybrene and spinoculated at 2 × 10^3RPM for 90min at 22°C. Cells were collected for subsequent assays and eGFP fluorescence determined using flow cytometric analysis 48 hours after transduction.

Statistical Analysis

Data were processed in GraphPad Prism 5.0 software. Statistical analysis for comparisons between two groups was performed with nonparametric unpaired Mann-Whitney U test. Survival data were analyzed with the Mantel-Cox log-rank test. * $p < 0.05$; ** $p < 0.01$; and *** $p < 0.005$ were considered as statistically significant.

CHAPTER SEVEN

References

1. Schofield, R. The relationship between the spleen colony-forming cell and the haemopoietic stem cell. *Blood Cells* **4**, 7-25 (1978).
2. Zhang, J. & Li, L. Stem cell niche: microenvironment and beyond. *J Biol Chem* **283**, 9499-9503 (2008).
3. Jagasia, M.*, et al.* Risk factors for acute GVHD and survival after hematopoietic cell transplantation. *Blood* **119**, 296-307 (2012).
4. Korngold, R. & Sprent, J. Lethal graft-versus-host disease after bone marrow transplantation across minor histocompatibility barriers in mice. Prevention by removing mature T cells from marrow. *J Exp Med* **148**, 1687-1698 (1978).
5. Lau, A., Villeneuve, N.F., Sun, Z., Wong, P.K. & Zhang, D.D. Dual roles of Nrf2 in cancer. *Pharmacol Res* **58**, 262-270 (2008).
6. Sporn, M.B. & Liby, K.T. NRF2 and cancer: the good, the bad and the importance of context. *Nature reviews. Cancer* **12**, 564-571 (2012).
7. Tsai, J.J.*, et al.* Nrf2 regulates haematopoietic stem cell function. *Nature cell biology* (2013).
8. Heasman, S.A., Zaitseva, L., Bowles, K.M., Rushworth, S.A. & Macewan, D.J. Protection of acute myeloid leukaemia cells from apoptosis induced by front-line chemotherapeutics is mediated by haem oxygenase-1. *Oncotarget* **2**, 658-668 (2011).

9. Rushworth, S.A., Bowles, K.M. & MacEwan, D.J. High basal nuclear levels of Nrf2 in acute myeloid leukemia reduces sensitivity to proteasome inhibitors. *Cancer Res* **71**, 1999-2009 (2011).

10. Rushworth, S.A. & MacEwan, D.J. HO-1 underlies resistance of AML cells to TNF-induced apoptosis. *Blood* **111**, 3793-3801 (2008).

11. Rushworth, S.A.*, et al.* The high Nrf2 expression in human acute myeloid leukemia is driven by NF-kappaB and underlies its chemo-resistance. *Blood* **120**, 5188-5198 (2012).

12. Weniger, M.A.*, et al.* Treatment-induced oxidative stress and cellular antioxidant capacity determine response to bortezomib in mantle cell lymphoma. *Clinical cancer research : an official journal of the American Association for Cancer Research* **17**, 5101-5112 (2011).

13. Wu, R.P.*, et al.* Nrf2 responses and the therapeutic selectivity of electrophilic compounds in chronic lymphocytic leukemia. *Proc Natl Acad Sci U S A* **107**, 7479-7484 (2010).

14. Rockwell, C.E., Zhang, M., Fields, P.E. & Klaassen, C.D. Th2 skewing by activation of Nrf2 in CD4(+) T cells. *J Immunol* **188**, 1630-1637 (2012).

15. Morzadec, C.*, et al.* Nrf2 expression and activity in human T lymphocytes: stimulation by T cell receptor activation and priming by inorganic arsenic and tert-butylhydroquinone. *Free radical biology & medicine* **71**, 133-145 (2014).

16. Turley, A.E., Zagorski, J.W. & Rockwell, C.E. The Nrf2 activator tBHQ inhibits T cell activation of primary human CD4 T cells. *Cytokine* **71**, 289-295 (2015).

17. Zuniga-Pflucker, J.C. T-cell development made simple. *Nat Rev Immunol* **4**, 67-72 (2004).

18. Tzeng, Y.S.*, et al.* Loss of Cxcl12/Sdf-1 in adult mice decreases the quiescent state of hematopoietic stem/progenitor cells and alters the pattern of hematopoietic regeneration after myelosuppression. *Blood* **117**, 429-439 (2011).

19. Sugiyama, T., Kohara, H., Noda, M. & Nagasawa, T. Maintenance of the hematopoietic stem cell pool by CXCL12-CXCR4 chemokine signaling in bone marrow stromal cell niches. *Immunity* **25**, 977-988 (2006).

20. Nie, Y., Han, Y.C. & Zou, Y.R. CXCR4 is required for the quiescence of primitive hematopoietic cells. *J Exp Med* **205**, 777-783 (2008).

21. Hill, G.R. & Ferrara, J.L. The primacy of the gastrointestinal tract as a target organ of acute graft-versus-host disease: rationale for the use of cytokine shields in allogeneic bone marrow transplantation. *Blood* **95**, 2754-2759 (2000).

22. Gooley, T.A.*, et al.* Reduced mortality after allogeneic hematopoietic-cell transplantation. *The New England journal of medicine* **363**, 2091-2101 (2010).

23. Castilla-Llorente, C.*, et al.* Prognostic factors and outcomes of severe gastrointestinal GVHD after allogeneic hematopoietic cell transplantation. *Bone marrow transplantation* **49**, 966-971 (2014).

24. Seemayer, T.A., Lapp, W.S. & Bolande, R.P. Thymic involution in murine graft-versus-host reaction. Epithelial injury mimicking human thymic dysplasia. *The American journal of pathology* **88**, 119-134 (1977).

25. Lapp, W.S., Ghayur, T., Mendes, M., Seddik, M. & Seemayer, T.A. The functional and histological basis for graft-versus-host-induced immunosuppression. *Immunological reviews* **88**, 107-133 (1985).

26. Krenger, W., Rossi, S., Piali, L. & Hollander, G.A. Thymic atrophy in murine acute graft-versus-host disease is effected by impaired cell cycle progression of host pro-T and pre-T cells. *Blood* **96**, 347-354 (2000).

27. Na, I.K.*, et al.* The cytolytic molecules Fas ligand and TRAIL are required for murine thymic graft-versus-host disease. *J Clin Invest* **120**, 343-356 (2010).

28. Panoskaltsis-Mortari, A.*, et al.* In vivo imaging of graft-versus-host-disease in mice. *Blood* **103**, 3590-3598 (2004).

29. Beilhack, A.*, et al.* In vivo analyses of early events in acute graft-versus-host disease reveal sequential infiltration of T-cell subsets. *Blood* **106**, 1113-1122 (2005).

30. Beilhack, A.*, et al.* Prevention of acute graft-versus-host disease by blocking T-cell entry to secondary lymphoid organs. *Blood* **111**, 2919-2928 (2008).

31. Na, I.K.*, et al.* Concurrent visualization of trafficking, expansion, and activation of T lymphocytes and T-cell precursors in vivo. *Blood* **116**, e18-25 (2010).

32. Brochu, S., Rioux-Masse, B., Roy, J., Roy, D.C. & Perreault, C. Massive activation-induced cell death of alloreactive T cells with apoptosis of

bystander postthymic T cells prevents immune reconstitution in mice with graft-versus-host disease. *Blood* **94**, 390-400 (1999).

33. Hashimoto, D.*, et al.* FTY720 enhances the activation-induced apoptosis of donor T cells and modulates graft-versus-host disease. *European journal of immunology* **37**, 271-281 (2007).

34. Campbell, D.J. & Butcher, E.C. Rapid acquisition of tissue-specific homing phenotypes by CD4(+) T cells activated in cutaneous or mucosal lymphoid tissues. *J Exp Med* **195**, 135-141 (2002).

35. Stagg, A.J., Kamm, M.A. & Knight, S.C. Intestinal dendritic cells increase T cell expression of alpha4beta7 integrin. *European journal of immunology* **32**, 1445-1454 (2002).

36. Mora, J.R.*, et al.* Selective imprinting of gut-homing T cells by Peyer's patch dendritic cells. *Nature* **424**, 88-93 (2003).

37. Johansson-Lindbom, B.*, et al.* Selective generation of gut tropic T cells in gut-associated lymphoid tissue (GALT): requirement for GALT dendritic cells and adjuvant. *J Exp Med* **198**, 963-969 (2003).

38. Mora, J.R.*, et al.* Reciprocal and dynamic control of CD8 T cell homing by dendritic cells from skin- and gut-associated lymphoid tissues. *J Exp Med* **201**, 303-316 (2005).

39. Picker, L.J.*, et al.* Control of lymphocyte recirculation in man. II. Differential regulation of the cutaneous lymphocyte-associated antigen, a tissue-selective homing receptor for skin-homing T cells. *J Immunol* **150**, 1122-1136 (1993).

40. Lin, X., *et al.* Advances in distinguishing natural from induced Foxp3(+) regulatory T cells. *International journal of clinical and experimental pathology* **6**, 116-123 (2013).

41. Kim, H.J., *et al.* Stable inhibitory activity of regulatory T cells requires the transcription factor Helios. *Science* **350**, 334-339 (2015).

42. Sebastian, M., *et al.* Helios Controls a Limited Subset of Regulatory T Cell Functions. *J Immunol* **196**, 144-155 (2016).

43. Myrick, C., *et al.* Linkage analysis of variations in CD4:CD8 T cell subsets between C57BL/6 and DBA/2. *Genes and immunity* **3**, 144-150 (2002).

44. Edinger, M., *et al.* CD4+CD25+ regulatory T cells preserve graft-versus-tumor activity while inhibiting graft-versus-host disease after bone marrow transplantation. *Nature medicine* **9**, 1144-1150 (2003).

45. Wong, P. & Pamer, E.G. Feedback regulation of pathogen-specific T cell priming. *Immunity* **18**, 499-511 (2003).

46. Tran, I.T., *et al.* Blockade of individual Notch ligands and receptors controls graft-versus-host disease. *J Clin Invest* **123**, 1590-1604 (2013).

47. Ponomarev, V., *et al.* A novel triple-modality reporter gene for whole-body fluorescent, bioluminescent, and nuclear noninvasive imaging. *European journal of nuclear medicine and molecular imaging* **31**, 740-751 (2004).

48. Motohashi, H., *et al.* NF-E2 domination over Nrf2 promotes ROS accumulation and megakaryocytic maturation. *Blood* **115**, 677-686 (2010).

49. Kuroha, T.*, et al.* Ablation of Nrf2 function does not increase the erythroid or megakaryocytic cell lineage dysfunction caused by p45 NF-E2 gene disruption. *J Biochem* **123**, 376-379 (1998).

50. Chan, K., Lu, R., Chang, J.C. & Kan, Y.W. NRF2, a member of the NFE2 family of transcription factors, is not essential for murine erythropoiesis, growth, and development. *Proc Natl Acad Sci U S A* **93**, 13943-13948 (1996).

51. Tothova, Z.*, et al.* FoxOs are critical mediators of hematopoietic stem cell resistance to physiologic oxidative stress. *Cell* **128**, 325-339 (2007).

52. Owusu-Ansah, E. & Banerjee, U. Reactive oxygen species prime Drosophila haematopoietic progenitors for differentiation. *Nature* **461**, 537-541 (2009).

53. Juntilla, M.M.*, et al.* AKT1 and AKT2 maintain hematopoietic stem cell function by regulating reactive oxygen species. *Blood* **115**, 4030-4038 (2010).

54. Ito, K.*, et al.* Reactive oxygen species act through p38 MAPK to limit the lifespan of hematopoietic stem cells. *Nat Med* **12**, 446-451 (2006).

55. Banning, A., Deubel, S., Kluth, D., Zhou, Z. & Brigelius-Flohe, R. The GI-GPx gene is a target for Nrf2. *Mol Cell Biol* **25**, 4914-4923 (2005).

56. Tullet, J.M.*, et al.* Direct inhibition of the longevity-promoting factor SKN-1 by insulin-like signaling in C. elegans. *Cell* **132**, 1025-1038 (2008).

57. Papaconstantinou, J. Insulin/IGF-1 and ROS signaling pathway cross-talk in aging and longevity determination. *Mol Cell Endocrinol* **299**, 89-100 (2009).

58. Geiger, H. & Rudolph, K.L. Aging in the lympho-hematopoietic stem cell compartment. *Trends Immunol* **30**, 360-365 (2009).

59. Hochmuth, C.E., Biteau, B., Bohmann, D. & Jasper, H. Redox regulation by Keap1 and Nrf2 controls intestinal stem cell proliferation in Drosophila. *Cell Stem Cell* **8**, 188-199 (2011).

60. Kang, K.W., Cho, M.K., Lee, C.H. & Kim, S.G. Activation of phosphatidylinositol 3-kinase and Akt by tert-butylhydroquinone is responsible for antioxidant response element-mediated rGSTA2 induction in H4IIE cells. *Molecular pharmacology* **59**, 1147-1156 (2001).

61. Bahia, P.K.*, et al.* Neuroprotective effects of phenolic antioxidant tBHQ associate with inhibition of FoxO3a nuclear translocation and activity. *Journal of neurochemistry* **123**, 182-191 (2012).

62. Zhang, Y.*, et al.* The antioxidant compound tert-butylhydroquinone activates Akt in myocardium, suppresses apoptosis and ameliorates pressure overload-induced cardiac dysfunction. *Scientific reports* **5**, 13005 (2015).

63. Waldman, E.*, et al.* Absence of beta7 integrin results in less graft-versus-host disease because of decreased homing of alloreactive T cells to intestine. *Blood* **107**, 1703-1711 (2006).

64. Petrovic, A.*, et al.* LPAM (alpha 4 beta 7 integrin) is an important homing integrin on alloreactive T cells in the development of intestinal graft-versus-host disease. *Blood* **103**, 1542-1547 (2004).

65. Hanash, A.M. & Levy, R.B. Donor CD4+CD25+ T cells promote engraftment and tolerance following MHC-mismatched hematopoietic cell transplantation. *Blood* **105**, 1828-1836 (2005).

66. Nguyen, V.H.*, et al.* The impact of regulatory T cells on T-cell immunity following hematopoietic cell transplantation. *Blood* **111**, 945-953 (2008).

67. Zakrzewski, J.L.*, et al.* Adoptive transfer of T-cell precursors enhances T-cell reconstitution after allogeneic hematopoietic stem cell transplantation. *Nat Med* **12**, 1039-1047 (2006).

68. Hayashi, H. & Kume, T. Forkhead transcription factors regulate expression of the chemokine receptor CXCR4 in endothelial cells and CXCL12-induced cell migration. *Biochem Biophys Res Commun* **367**, 584-589 (2008).